ISSN 8755-6839

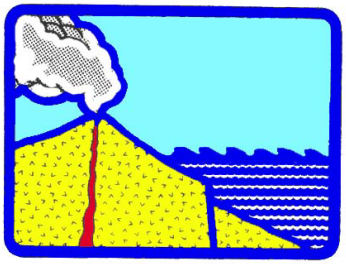

SCIENCE OF
TSUNAMI HAZARDS

The International Journal of The Tsunami Society

Volume 21 Number 3 Published Electronically 2003

ASSESSING TSUNAMI HAZARD ALONG THE NEW ZEALAND COAST 137
Roy A. Walters
National Institute of Water and Atmospheric Research, Christchurch, New Zealand
James Goff
GeoEnvironmental Consultants, Lyttleton, New Zealand

BASIC RELATIONS BETWEEN TSUNAMI CALCULATIONS AND THEIR PHYSICS - II 154
Zygmunt Kowalik
Institute of Marine Science, University of Alaska, Fairbanks, Alaska, USA

copyright © 2003
THE TSUNAMI SOCIETY
P. O. Box 37970,
Honolulu, HI 96817, USA

WWW.STHJOURNAL.ORG

OBJECTIVE: **The Tsunami Society** publishes this journal to increase and disseminate knowledge about tsunamis and their hazards.

DISCLAIMER: Although these articles have been technically reviewed by peers, **The Tsunami Society** is not responsible for the veracity of any statement, opinion or consequences.

EDITORIAL STAFF

Dr. Charles Mader, Editor
Mader Consulting Co.
1049 Kamehame Dr., Honolulu, HI. 96825-2860, USA

EDITORIAL BOARD

Mr. George Curtis, University of Hawaii - Hilo
Dr. Zygmunt Kowalik, University of Alaska
Dr. Tad S. Murty, Baird and Associates - Ottawa
Dr. Yurii Shokin, Novosibirsk
Mr. Thomas Sokolowski, Alaska Tsunami Warning Center
Professor Stefano Tinti, University of Bologna

TSUNAMI SOCIETY OFFICERS

Dr. Barbara H. Keating, President
Dr. Tad S. Murty, Vice President
Dr. Charles McCreery, Secretary
Dr. Laura Kong, Treasurer

Submit manuscripts of articles, notes or letters to the Editor. If an article is accepted for publication the author(s) must submit a scan ready manuscript, a TeX or a PDF file in the journal format. Issues of the journal are published electronically in PDF format. The journal issues for 2002 are available at

http://www.sthjournal.org.

Tsunami Society members will be advised by e-mail when a new issue is available and the address for access. There are no page charges or reprints for authors.

Permission to use figures, tables and brief excerpts from this journal in scientific and educational works is hereby granted provided that the source is acknowledged.

Previous volumes of the journal are available in PDF format at

http://epubs.lanl.gov/tsunami/

and on a CD-ROM from the Society to Tsunami Society members.

ISSN 8755-6839 **http://www.sthjournal.org**

Published Electronically by The Tsunami Society in Honolulu, Hawaii, USA

ASSESSING TSUNAMI HAZARD ALONG THE NEW ZEALAND COAST

Roy A. Walters
National Institute of Water & Atmospheric Research Ltd.
PO Box 8602
Christchurch, New Zealand
r.walters@niwa.cri.nz

James Goff
GeoEnvironmental Consultants
11 The Terrace
Governors Bay
Lyttleton RD1, New Zealand
geoenv@xtra.co.nz

ABSTRACT

An assessment is made for tsunami hazards along the New Zealand coast by searching for long-wave resonances for the range of periods spanned by tsunami and short-period storm surges. To accomplish this, a high-resolution model of the southwest Pacific is used to simulate the effects of these waves in an oceanic domain extending over 40° in latitude and 50° in longitude. This paper describes the results of such a simulation for waves with a period in the range of 15 to 300 minutes. The locations where wave resonances occur are compared with historical and geological evidence in order to evaluate the concurrence of the locations. A search of geological data was undertaken, and the results of palaeotsunami studies were compared with model predictions to determine the general utility of using resonance patterns to assess tsunami hazards.

Introduction

Tsunami and storm-surge events have occurred relatively frequently along the coast of New Zealand in historic times (de Lange & Fraser 1999; de Lange in press). Both are temporary oscillations of sea level with periods longer than wind waves and shorter than tides for tsunami, and shorter than a few days for storm surge. They can cause coastal flooding, erosion, and loss of life in extreme events, and therefore can be significant coastal hazards. In the prehistoric record the resolution of events is not as detailed, although large coastal inundations, or Catastrophic Saltwater Inundations (CSI), have been identified (e.g. Goff et al., 2000). In the case of tsunami and possibly storm-surge events, it is estimated that wave runup in excess of about 5m are needed to leave a "recognisable" deposit (Lowe and de Lange, 2000). Relating these events to inundation by either tsunami or storm surge often requires detailed examination, but this type of data can prove to be extremely useful for comparing with and complementing hydrodynamic models (Goff et al., 2001a).

Tsunami can be classified by the distance from their source to the area of impact; i.e., local and remote tsunami. Locally generated tsunami have short warning times and relatively short wave periods; remote tsunami have longer warning times and relatively long periods. Typical periods for tsunami range from 15 minutes for locally generated tsunami to several hours for remote tsunami. Typical runup height for tsunami range up to 15 m at the coast, although most are much smaller. Storm surges on the other hand are caused by variations in barometric pressure and wind stress over the ocean. Decreasing barometric pressure causes an inverse barometer effect where sea level rises. This is usually a slow and large-scale effect and thus does not usually generate waves in the frequency range typical of tsunami. However, there can be short-period meteorological events (such as meteorological tsunami – rissaga) with time-scales of a few hours that may be important (de Lange, in press). Wind stress on the other hand has a wide range of time-scales and causes coastal sea-level setup as well as wind waves, where the setup depends on the wind direction, strength, and wave height. Storm surge periods range from several hours to several days. Typical heights for storm surge alone range up to 1.0 m along the coast of New Zealand, although most are usually less than 0.5 m (Bell et al., 2000). Wind waves, on the other hand, can be quite large, producing wave setup and wave runup of several meters in height.

In the end, the runup of tsunami and storm-generated waves depends on the initial or incident amplitude and direction, the wave period, and how the wave interacts with the ocean and shoreline topography. Where a harbour or coastal bay resonates with a similar period to the incident wave, large amplification of incident waves can be expected. The ability to differentiate between tsunami and storm deposits is becoming increasingly significant as researchers are now able to identify CSIs that do not have a "recognisable" or visible deposit. This is being achieved through the use of techniques such as micropalaeontological and geochemical analyses (Goff et al., 2001b). The increasing ability to identify smaller events means that it is more likely that it will be necessary to effectively differentiate between tsunami and storms. This becomes important when resonance modelling identifies areas of coastline susceptible to both tsunami and storm inundation.

The objective of the work presented here is to assess coastal tsunami hazards by searching for resonances along the New Zealand coast for the range of periods spanned by tsunami. These locations are compared with historic and geological evidence (Figure 1) in order to evaluate the

corroboration between the sets of information. To accomplish this, a high-resolution hydrodynamic model was used to simulate the effects of these waves in the southwest Pacific Ocean. This paper describes the results of such a simulation for regular waves with a period in the range of 15 minutes to 5 hours. A search of geological data was undertaken, and the results of palaeotsunami studies were compared with model predictions to determine the general utility of using resonance patterns to assess tsunami hazards and to focus the search for palaeotsunami deposits.

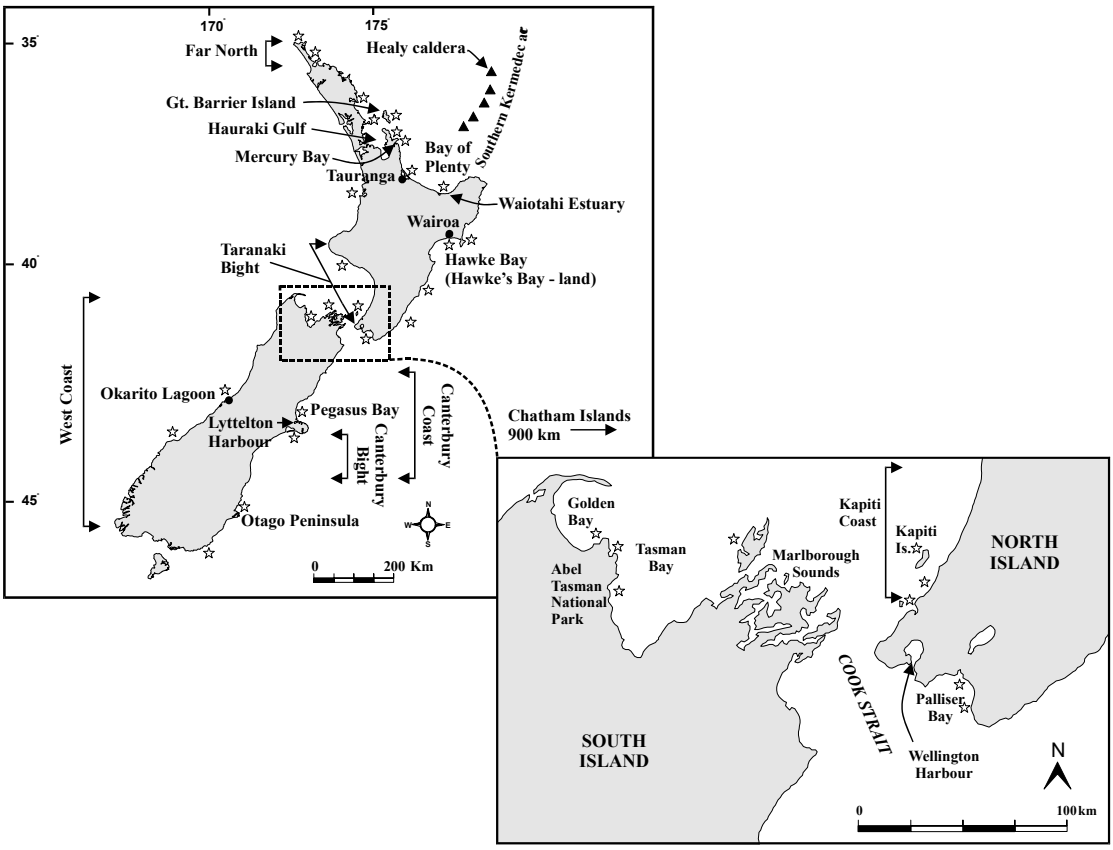

Figure 1: New Zealand locations mentioned in the text (star symbol indicates approximate location of confirmed or possible palaeotsunami deposits)

Methods

1. Model simulations

A high-resolution numerical model for tides around New Zealand has been developed by Walters et al (2001). Here the model is used to simulate continuous waves with periods in the range of 15 to 300 minutes rather than tidal periods. The model is based on the 2-dimensional shallow-water equations with all the non-linear terms retained. Through a choice of appropriate discretisations for time and space, this model is both robust and efficient. This property has

allowed calculations using a high-resolution grid and allowed considerable sensitivity testing. Details about the development of the numerical model were given by Walters (1987, 1992) and will not be repeated here. A summary of the model formulation is as follows.

- The numerical model is based on the 2-dimensional shallow water equations, where the Boussinesq and hydrostatic approximations are used. The resulting equations have sea level and depth-averaged velocity as the dependent variables.

- The dependent variables are expressed in terms of a harmonic expansion of constituents of various frequencies. Non-linear terms are expressed as simple frequency sums and differences for the advection and wave drift-terms, and by a series expansion for the bottom friction term. The expansion of the quadratic bottom friction term is a generalised expansion that does not depend on a dominant frequency. In this paper, a single wave frequency is used and the higher harmonics generated are ignored.

- After harmonic decomposition, the governing equations are expressed in the form of a continuity equation and a horizontal momentum equation. For a number of reasons relating to accuracy, stability, and efficiency, the continuity equation is written as an equation of the Helmholz type. This equation formulation has the advantage that the solution for sea level and the solution for velocity are not coupled, which increases computational efficiency. In practice, a matrix equation for sea level is solved first, followed by a point-wise solution for velocity that uses these sea level values.

- The spatial part of the governing equations is discretised using finite element methods. The boundary conditions are zero normal flow at land boundaries (a natural boundary condition of the finite element formulation), incident wave amplitude and phase specified along one side of the open ocean boundary, and radiation conditions along all sides of the open ocean boundary. This choice allows passing a regular wave inwards through either the north, south, east, or west boundary, and allowing it to radiate out through all the boundaries. Thus the solution is not contaminated by waves artificially reflecting off the open boundaries. The results presented here are for a wave incident from the east of the New Zealand region, such as a tsunami generated on the west coast of South America.

- The numerical simulations include waves with 14 different periods, ranging from 15 minutes to 5 hours (15, 18, 24, 30, 45, 60, 75, 90, 120, 150, 180, 210, 240, and 300 minutes). The wave periods do not interact. The amplitude of the incident waves is specified as 0.01 m, with 0 degrees phase, along the eastern boundary.

The region around New Zealand has been discretised into a finite element grid with triangular elements using the grid generation software of Henry & Walters (1993). The grid contains 32065 nodes and 59700 elements (Figure 2). The horizontal spacing between computational nodes varies from 98 km near the ocean boundaries to 300 m near the coast. The grid encompasses the area between 156.75 and 210° E, and 23.75 and 65° S. The bathymetric data were acquired from three sources: Royal New Zealand Navy Hydrographic Office, National

Institute of Water and Atmospheric Research (NIWA) bathymetry archive, and Smith & Sandwell (1997).

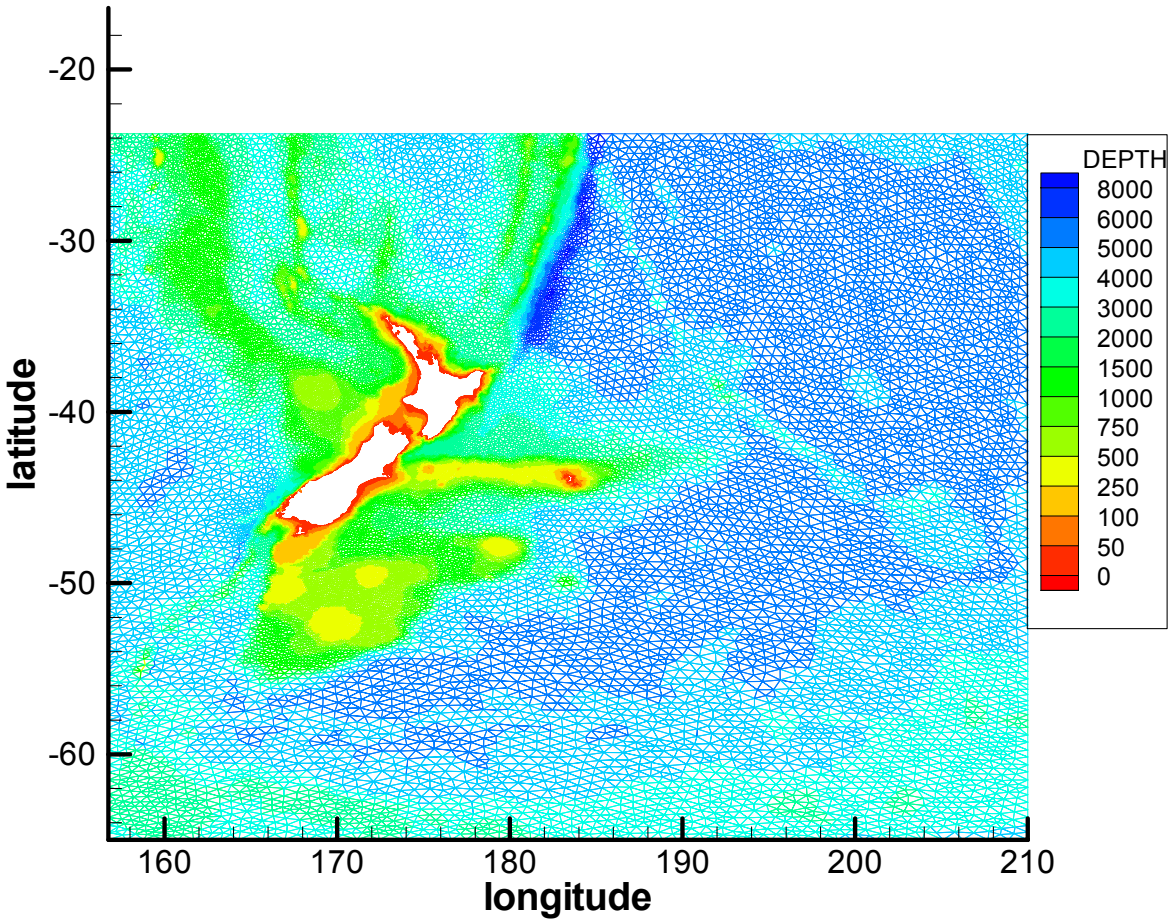

Figure 2: Finite element model grid, colour coded for water depth.

All the concepts above were developed based on the idea of a continuous wave train such as that produced by the numerical model. Then how is this related to a finite wave train produced during a storm or tsunami event? Typically, these events produce from a few to ten or so waves that interact when they approach the shoreline. Thus the wave patterns that are noted in the continuous simulations and are far from the coast would probably not be observed for finite length events because the wave train would not interact with itself over such large distance. However, near the coast these patterns would appear as a transient feature as the wave train passed. Therefore the analysis with a continuous wave field provides an efficient way to explore for resonances. Areas of special interest can be examined in future work with transient models.

2. Geological Record

A definitive identification of a palaeotsunami deposit hinges on the recognition of as many diagnostic characteristics as possible (Table 1). However, it is still important to understand the context or palaeoenvironmental conditions at the time of deposition (e.g. Witter et al., 2001) and to be able to identify a probable tsunami source if possible. Even a standard conception that a palaeotsunami deposit represents 'a deposit out of place' (e.g. a sand layer sandwiched between peat) must be treated with caution since this visible identification is dependent upon the nature of both the material available for entrainment and the depositional environment. Therefore, perhaps counter-intuitively, a mud layer in sand can represent a palaeotsunami (or palaeostorm) deposit (Goff and Chagué-Goff, 1999).

The absence of some diagnostic characteristics does not negate a palaeotsunami interpretation, but rather it can be indicative of the particular context. For example, the absence of buried soil or vascular plants might mean that either the underlying material was devoid of vegetation, or that the nature of inundation removed the material prior to deposition of 'clean' sediment. Hence it is useful to understand palaeoenvironmental conditions at the time of deposition. In general terms, if the study site was relatively exposed to the sea it is possible that the last inundation removed evidence of earlier events and also has a limited number of potential diagnostic characteristics. A more sheltered, low energy coastal wetland would be more likely to preserve evidence of multiple inundations and have more diagnostic characteristics (Goff et al., 2001b).

The New Zealand palaeotsunami record currently consists of "recognisable" deposits laid down by waves running up probably 5.0 m or higher above mean sea level (Lowe and de Lange, 2000). However, in most cases it is possible to differentiate between relative event magnitudes based upon the palaeogeomorphology of the setting, at least in the broad categories of '>5.0-10.0 m (large)' and '>10.0 m (extreme)' (Goff et al., 2001a). The latter category should be considered a catch-all for events greater than 10.0 m. In New Zealand the record of these extreme events ranges in height up to at least 32.0 metres above mean sea level (Nichol et al., 2002), although this should not be considered a maximum. The New Zealand record is far from complete and will continue to grow as more sites are studied and more and better analytical techniques are developed. However, there is sufficient information available now to undertake a national comparison between model results and geological data.

Results and Discussion

It is important to recall that the coastal effect of a tsunami depends on both the source characteristics and the coastal response characteristics. For remote tsunami, maximum amplitudes and spectral content of the waves are more or less known from historic data. This information combined with admittance information derived from the response patterns leads to reasonable estimation of effects. For local tsunami, the situation is very different. In particular, the source characteristics are not well defined along the New Zealand coast. Hence, resonance patterns may be indicative of a tsunami hazard but the lack of a source makes the issue moot. On the other

hand, a large local source can make the resonance analysis of little predictive value and a localisd transient model would be more appropriate.

In presenting the results, we will start with a general overview of the resonance characteristics of the east coast of New Zealand. We then place these patterns in the context of historic data, and show generally good correspondence between resonance patterns and observations. Then we subdivide the coastline further and consider the relation between the resonance patterns and palaeotsunami data.

As expected, resonance patterns show an increase in wavelength with increasing period of the incident waves. Then as the wavelength changes, the coastal response changes in predictable ways (Walters, 2002). For the simulations presented here, the wave propagates in from the eastern boundary and is allowed to radiate out through all the boundaries. An examination of the results for the entire grid shows that the radiation conditions are effective in that little outgoing wave energy is reflected back into the modelled area, as expected in reality. The wave refracts around the north and south ends of New Zealand and propagates through Cook Strait. Thus this one scenario yields resonance characteristics for everywhere except the west coast of both North and South Island.

In these results, the pattern of amplitudes is of primary importance, not the exact magnitudes. In essence, the spatial pattern shows the areas of large amplification of the incident wave. These areas are then potential "hot spots" for tsunami resonance and are therefore hazardous parts of the coast. The actual amplitude that would be observed depends upon the amplitude of the incident wave, which is in turn dependent on the details of the generation of the wave. Here, we look at the broader pattern of resonance (and by implication inundation hazard) rather than the details of individual events.

These results are displayed in an area just large enough to include all the coastline of New Zealand and Chatham Island (approximately 164 to 185° E and 31 to 51° S, Figure 3, 4, and 5). The entire model grid and underlying bathymetry for this area is shown in Figure 2. Note the extensive shelf in some areas such as the Chatham Rise to the east of South Island, as well as the narrow continental shelf in other areas such as east of North Island. When the waves incident from the ocean pass over the continental shelf, the wavelength decreases and amplitude increases.

Typical results for decreasing wave periods are shown in Figures 3, 4, and 5 (150, 60, and 24 minute periods). For areas with resonances, the sequence of figures shown in Walters (2002) gives a distinct sequence of patterns. For periods larger than the largest resonance period (fundamental frequency), there is little amplification. As the decreasing period approaches the resonance period of a particular embayment or bight, the amplitude increases to a maximum with a spatial pattern that contains a single maximum in that area. As the period decreases below the resonance, the amplitude decreases until it approaches the next resonance (first harmonic) where it again increases and shows a pattern with two maxima in the embayment. This behaviour is repeated for all the remaining harmonics in the range of wave periods used here.

The spatial patterns replicate the observed patterns in historic tsunami. For instance, consider the 1960 Chilean tsunami, one of the most extensive tsunami recorded in New Zealand (de Lange and Healy, 1986; Heath, 1976). The resonance pattern predicted by the model in Pegasus Bay and Lyttleton Harbour indicates a strong peak at around 150 minutes and the Chatham Rise tends to act as a waveguide directed at the Canterbury coast (Walters, 2002). The time-series data also show a similar amplification of the low frequency part of the spectrum in the

1960 tsunami (Heath, 1976) and in the 2001 Peru tsunami (Goring, 2002). On the other hand there is little response around the Otago Peninsula either in the model results or sea-level data. Wellington Harbour responded in terms of its dominant oscillation modes, one with a period of about 160 minutes and several with periods around 30 minutes as shown for example in Figure 5 (Heath, 1976; Abraham, 1997; Walters, 2002). The response at Tauranga (Heath, 1976) and Hawke Bay (de Lange and Healy, 1986) also follow the predicted response patterns with wave periods near the resonance peaks of 60 minutes and 150 minutes and shorter, respectively. Finally, records from Mercury Bay (unpublished data) show there was a 40 minute resonance as the patterns from the model would predict. To a large degree, these resonance patterns reflect the actual response to remote tsunami.

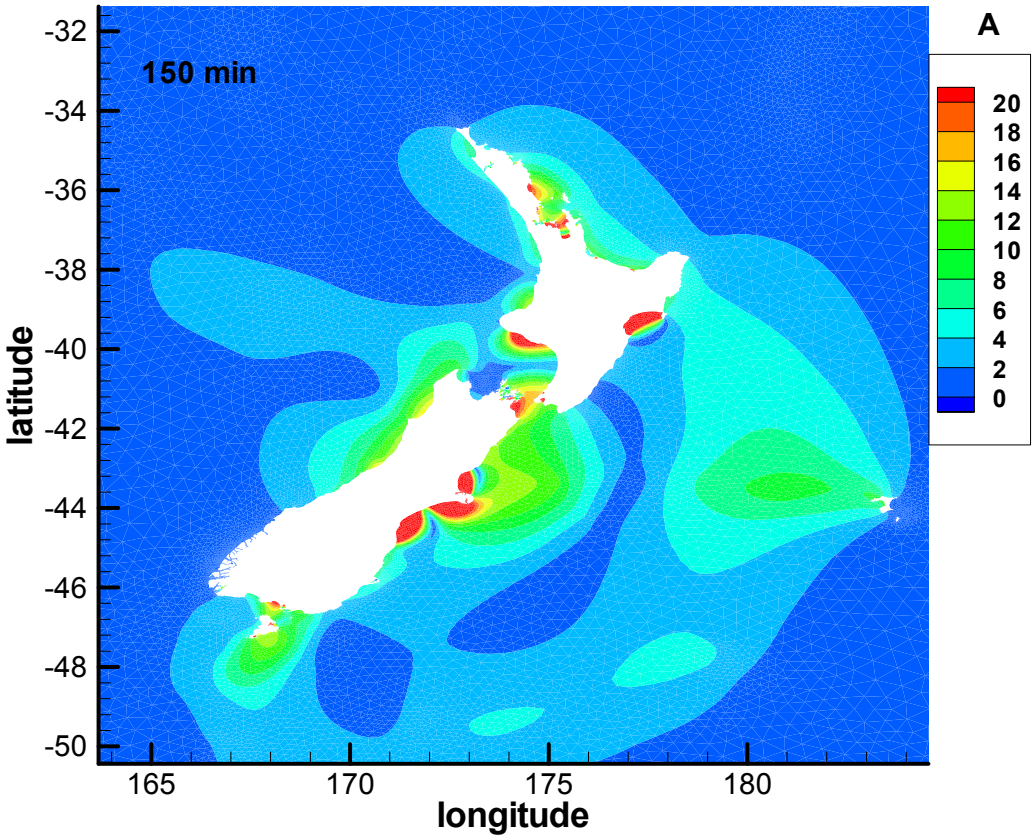

Figure 3: Resonance pattern for a wave with a period of 150 minutes, incident from the eastern boundary. The amplification factor, A, is the wave amplitude at a point divided by the amplitude of the incident wave at the eastern boundary.

There is currently no comparable palaeotsunami dataset to that of the historic record thus making it more difficult to analyse and interpret in detail. Therefore, a brief summary of palaeotsunami work to date is given in Table 2, and this should serve as a guide to the

discussions below.

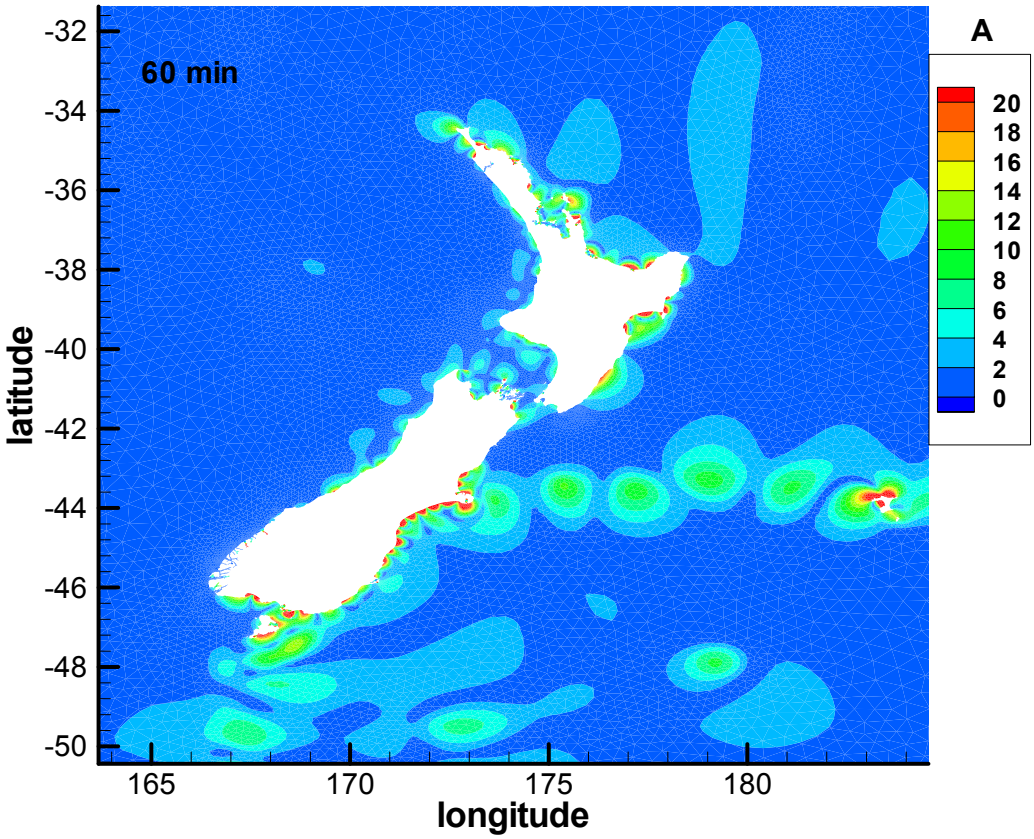

Figure 4: **Resonance pattern for a wave with a period of 60 minutes, incident from the eastern boundary. The amplification factor, A, is the wave amplitude at a point divided by the amplitude of the incident wave at the eastern boundary.**

Analysis of geological research carried out to date indicates that there have been several large palaeotsunami (probable wave heights of 5-15 m) dating back to about 6300 years BP (Goff et al., 2001b; Goff and McFadgen, 2002). The full areal extent of these is still unclear, but of particular interest are the more recent ones of approximately 200AD, 1220AD and 1450AD. The first coincides with the Taupo eruption (Lowe and de Lange, 2000) and the last two with several large, local fault ruptures (Goff et al., 2000). Furthermore, in 1450AD, many prehistoric Maori coastal settlements around the country were inundated and subsequently abandoned (Goff and McFadgen, 2002). These prehistoric coastal settlements serve as a guide for local inundation heights and potential resonances. The return period for these large, locally-generated palaeotsunami is believed to be about once every 500 years (Goff and Chagué-Goff, 2001; Goff et al, 2001b).

It is believed that all of these earlier palaeotsunami deposits are from local tsunami sources so that it is best to compare the geological data with resonance patterns with relatively short wave period. With this in mind we have chosen the 60-minute nationwide pattern and 24-minute Cook Strait region pattern as a focus (Figures 4 and 5).

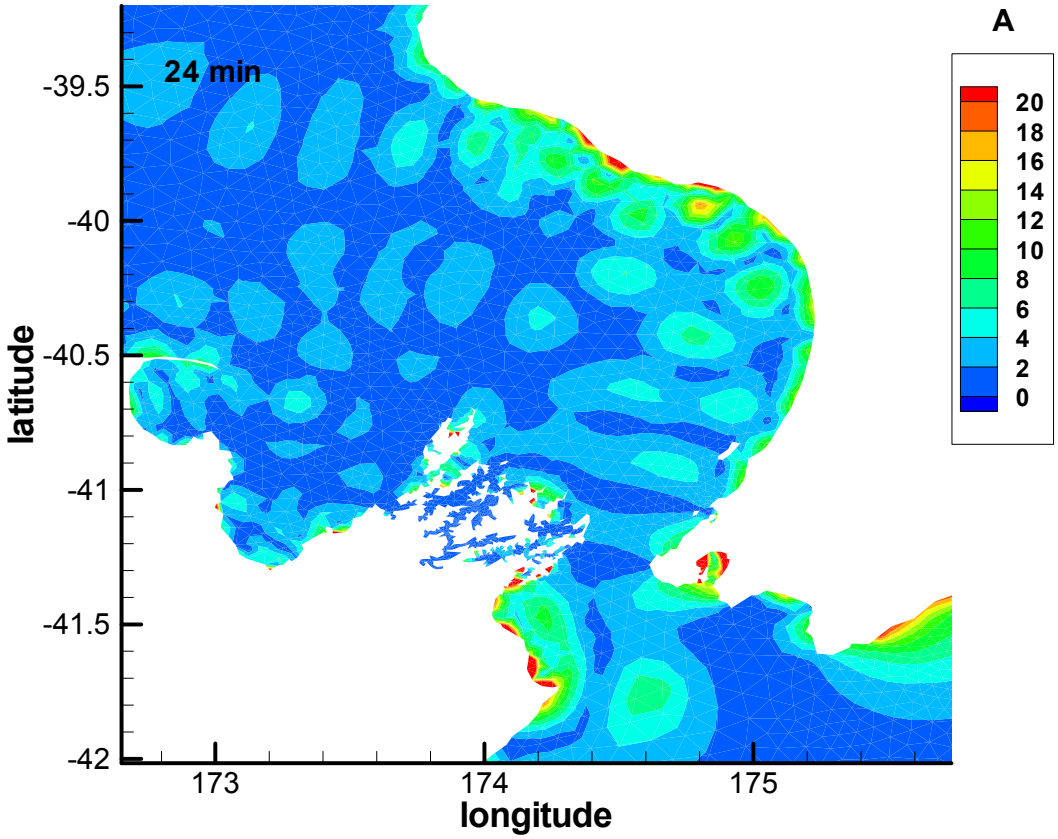

Figure 5: Resonance pattern in the Cook Strait region for a wave with a period of 24 minutes, incident from the eastern boundary.

Looking along the length of the east coast there appears to be considerable agreement between the location of palaeotsunami deposits and resonance patterns (Figures 1, 4, and 5). Of particular note are deposits reported from the Far North, the east coast of Great Barrier Island, Wairoa, Palliser Bay (two sites on the northern and eastern sides), Kapiti Island, Abel Tasman National Park, Pegasus Bay, and the Canterbury Bight. These have all been studied in some degree of detail. Other locations along the east coast where possible palaeotsunami deposits have been recorded, but not fully investigated, include sites on the mainland coast just north of Great Barrier Island, in the Bay of Plenty (Tauranga and Waiotahi Estuary), western Marlborough Sounds, and south of the Canterbury Bight. Several other confirmed or possible palaeotsunami deposits have been reported from other parts of the country, such as Okarito Lagoon and the Taranaki Bight on the west coast. While these are not the focus of this paper it is worth noting

that all the locations shown in Figure 1 correspond to areas with short-period resonances (Walters, 2002).

The correspondence between short-period resonances and palaeotsunami deposits seems to point towards the possibility that all the deposits found so far in New Zealand are probably from events with a local source. However, as mentioned above, the 1960 Chilean tsunami had strong resonance patterns in Pegasus Bay, Tauranga, Hawke Bay and the western Bay of Plenty (Mercury Bay). Therefore, distant sources cannot be completely discounted, and indeed, at 150 minutes there are general resonances in many of the areas where palaeotsunami deposits have been found such as Hawke Bay, Taranaki Bight, Marlborough Sounds, Pegasus Bay, and the Canterbury Bight.

Distantly-generated tsunami show no resonance at 150 minutes in the northern part of the North Island except in the Hauraki Gulf (Figure 3). There are numerous resonances at shorter wave periods that might also be correlated with distantly-generated tsunami, although the nature and extent of the palaeotsunami deposits found in this region (from the Far North to the eastern Bay of Plenty, informally named the "tsunami crescent") suggest that they are most likely to relate to events from a local source. Several near-contemporaneous (15th Century) palaeotsunami deposits have also been reported from other parts of the country, and have been linked with a series of tsunamigenic events including several large fault ruptures and submarine volcanic eruptions (Figure 1, Table 2, refer to Goff and McFadgen, 2002 for full details of the 15th century events).

The contemporaneous deposits of the tsunami crescent must have been laid down by a tsunami with a local source sufficiently distant and large to affect the whole area. A logical source is submarine volcanism and/or associated earthquake activity in the vicinity of the Hikurangi trough, east of the southern Kermadec arc and 360 km east–southeast of Great Barrier Island (Figure 1). This is a seismically active area that has experienced a minimum of 21 large (Mag. 7.3 or greater) paleoseismic events during the past 2.5 ka (Berryman et al., 1989). An equally logical source is the southern Kermadec arc that is comprised of at least 13 modern submarine volcanoes between 34^{o}50'S and 36^{o}50'S (Figure 1) (Wright and Gamble, 1999). Of these volcanoes, the Healy caldera is a strong candidate for tsunami generation. A probable 15th Century eruption (contemporaneous with the palaeotsunami deposits) was pyroclastic and the associated caldera collapse in 550-1000 m water depth was catastrophic and possibly tsunamigenic (Wright et al., in press).

Confirmed or possible palaeotsunami deposits that are probably related to the Healy caldera collapse have been found in the Far North, on Great Barrier Island, on the mainland coast just north of Great Barrier Island, and in the Bay of Plenty (north-west, and south-west) (Figure 1). A comparison with the resonance patterns shows that in every palaeotsunami deposit location there is a corresponding short-period resonance. The resonance diagram also indicates other areas where resonance occurs, but where no geological studies have been undertaken, such as two areas in eastern Bay of Plenty, and one in eastern Hauraki Gulf (Figure 4). In this instance the resonance diagrams appear to serve as a guide for further palaeotsunami field studies.

If this comparison between palaeotsunami deposits and short period resonances is taken further, a superimposition of the nationwide palaeotsunami data indicates that there is considerable match-up between the model results and geological data, but there are other areas where the two do not coincide, such as parts of the west coast (Figures 1 and 4). It should be

noted that the resonance diagrams produced here are primarily related to remote events from the east. Some use can be made of these data for some locally-generated events from the east, but there is no consideration of either local or remote events from the west. Although a distant western or southern source is highly unlikely, there are numerous potential local sources including submarine faults and a steep continental shelf off the southwestern part of the country. While parts of a coastline may not resonate, this does not mean that a large, locally-generated tsunami will not catastrophically inundate the shoreline. Indeed, this appears to be the case for the West Coast, where co-seismic coastal subsidence also occurs in some places (Goff et al., 2001c).

Other problems are also found when attempting to match-up model and geological data. For example, in southern Hawke's Bay geological fieldwork has so far been unable to identify any palaeotsunami deposits (they have been found at Wairoa in the north of Hawke's Bay) and yet resonance is strong at both 60 and 150 minutes. This absence of data does not necessarily mean the absence of tsunami. It was not until after the mid 1990's and the first identification of palaeotsunami deposits in New Zealand that coastal research started to consider tsunami. Moreover, if a sufficiently large tsunami inundated the coastline, the appropriate type of depositional environment is required to preserve evidence of the event. For example, unless it is overtopped, a cliffed coastline such as southern Hawke's Bay is unlikely to preserve a palaeotsunami deposit. New Zealand's coast is about 18200 km long (Rouse et al., in press) and there are many areas where resonances occur and no geological work has been carried out. The absence of correspondence between the model and geological evidence may therefore simply be a function of a lack of data.

Conclusions

This paper summarises the methods and data used to obtain an accurate model for long wave propagation in a continental-shelf area of inherently complex interference patterns. Using this procedure, the spatial response pattern for waves with periods in the range of 15 to 300 minutes was explored. This has proven to be an efficient method to search for "hot spots" with large resonances and hence areas with potential tsunami risk.

The resonance patterns have been compared with existing historic and geological data. In general, there is good agreement between the resonance patterns and historical data for remote tsunami. Using the 1960 Chilean tsunami as an example, the amplitudes and wave periods at many locations along the east coast of New Zealand are in agreement with the strength and frequency of the resonance peaks. This indicates that the model results should provide a reliable index of risks associated with remote tsunami.

A comparison between the shorter-period resonance patterns and palaeotsunami data also shows a good match-up between the datasets, particularly in areas where there is some considerable geological detail such as within the Cook Strait area. This geological ground truth indicates the general utility of the model results, but also serves notice that additional information is needed for local sources.

There are also areas where the model does not match the geological data. There are several explanations for this, although it is most likely that geological records refer to locally generated events that are not within the scope of the resonance analysis. However because of the generally

excellent match-up around the coast, it is suggested that these areas must be considered in evaluating tsunami hazards.

Acknowledgments

Part of this project was funded by NSOF augmenting FRST-funded programme C01X0015 (Natural Physical Hazards affecting Coastal Margins and the Continental Shelf). GeoEnvironmental Consultants funded part of the geological research discussed in this paper. We are indebted to Rob Bell for his careful review of the manuscript.

References

Abraham, E.R.C. (1997): Seiche modes of Wellington Harbour, New Zealand. *New Zealand Journal of Marine and Freshwater Research 31*: 191–200.

Bell, R.G.; Goring, D.G. and de Lange, W.P. (2000). Sea level change and storm surges in the context of climate change. *IPENZ Transactions 27(1) – General*: 1–10. (Also on Web site: http://www.ipenz.org.nz/ipenz/publications/transactions/).

Berryman, K.R., Ota, Y., and Hull, A.G., (1989). Holocene paleoseismicity in the fold and thrust belt of the Hikurangi subduction zone, eastern North Island, New Zealand. *Tectonophysics* 163, 185– 195.

Chagué-Goff, C., Dawson, S., Goff, J.R., Zachariasen, J., Berryman, K.R., Garnett, D.L., Waldron, H.M. and Mildenhall, D.C. (2002). A tsunami (c. 6300 years BP) and other environmental changes, northern Hawke's Bay, New Zealand. *Sedimentary Geology 150*, 89-102.

Chagué-Goff, C. and Goff, J.R. (1999). Geochemical and sedimentological signature of catastrophic saltwater inundations (tsunami). *New Zealand. Quat. Aust. 17*, 38-48.

de Lange, W.P. (in press). Chapter 4: Tsunami and storm surge hazard in New Zealand. *In:* Rouse, H.L.; Goff, J.R. and Nichol, S. (eds.) The New Zealand Coast: Te Tai O Aotearoa. Daphne Brasnell Associates Ltd, Auckland.

de Lange, W.; Fraser, R.J. (1999). Overview of tsunami hazard in New Zealand. *Tephra 17*: 3–9.

de Lange, W.P.; Healy, T.R. (1986). New Zealand tsunamis 1840-1982. *New Zealand Journal of Geology and Geophysics 29*: 115-134.

Goff, J.R., Chagué-Goff, C. (1999). A Late Holocene record of environmental changes from coastal wetlands. Abel Tasman National Park. *New Zealand. Quat. Int. 56*, 39-51.

Goff, J.R. and Chagué-Goff, C. (2001). *Catastrophic events in New Zealand coastal environments.* Conservation Advisory Sciences Notes No. 333, Department of Conservation, Wellington, 16pp.

Goff, J.R. and McFadgen, B.G. (2002). Seismic driving of nationwide changes in geomorphology and prehistoric settlement – a 15th Century New Zealand example. *Quaternary Science Reviews 21/22*, 2313-2320.

Goff, J.R., Crozier, M., Sutherland, V., Cochran, U., and Shane, P. (1998). Possible tsunami deposits of the 1855 earthquake, North island, New Zealand. In: Stewart, I.S., Vita-Finzi, C. (Eds.). Coastal Tectonics. Geol. Soc. Spec. Pub. No. 133, pp. 353-374.

Goff, J.R., Rouse, H.L., Jones, S., Hayward, B., Cochran, U., McLea, W., Dickinson, W.W., Morley, M.S. (2000). Evidence for an earthquake and tsunami about 3100-3400 years ago, and other catastrophic saltwater inundations recorded in a coastal lagoon. *New Zealand. Mar. Geo. 171*, 233-251.

Goff, J.R., McFadgen, B.G., Chagué-Goff, C., Downes, G., Kozuch, M. and Bell, R. (2001a). Wellington Regional Tsunami Hazard Scoping Project. GeoEnvironmental Consultants Client Report GEO2001/20008/12. Wellington Regional Council Publication No. WRC/RP-T-01/23, 117pp. (http://www.wrc.govt.nz/pub/view_doc.cfm?id=468). ISBN 363.34909936.

Goff, J., Chagué-Goff, C. and Nichol, S. (2001b). Palaeotsunami deposits: A New Zealand perspective. *Sedimentary Geology*, 143, 1-6.

Goff, J., Nichol, S. and Chagué-Goff, C. (2001c). Environmental changes in Okarito Lagoon, Westland. GeoEnvironmental Consultants Client Report 20003. Department of Conservation Internal Series No. 3, 30pp.

Goring, D.G. (2002). Response of New Zealand waters to the Peru tsunami of 23 June 2001. *New Zealand Journal of Marine and Freshwater Research 36*: 225–232.

Heath, R.A. (1976). The response of several New Zealand harbours to the 1960 Chilean tsunami. *In:* Heath, R.A., Cresswell, M. (eds) Tsunami Research Symposium 1974. *Bulletin of the Royal Society of New Zealand 15*: 71–82.

Henry, R.F., and Walters, R.A. (1993). A geometrically-based automatic generator for irregular triangular networks. *Communications in Applied Numerical Methods 9*.

Lowe, D.J., and de Lange, W.P. (2000). Volcano-meteorological tsunamis, the c. AD 200 Taupo eruption (New Zealand) and the possibility of a global tsunami. *Holocene 10*, 401-407.

Nichol, S., Goff, J, Regnauld, H. and Lian, O. (2002). Tsunami deposit of possible volcanogenic origin, Henderson Bay, New Zealand. Poster. First Symposium on New Zealand-France Collaborative Research in Geosciences, Wellington, New Zealand. July 15-16.

Nichol, S.L., Lian, O.B., and Carter, C.H. (in press). Sheet-gravel evidence for a late Holocene tsunami run-up on beach dunes, Great Barrier Island, New Zealand. *Sedimentary Geology*.

Rouse, H.L., Goff, J.R. and Nichol, S. (in press). Introduction. *In:* Rouse, H.L., Goff, J.R. and Nichol, S. (eds.) *The coast of New Zealand: Te Tai O Aotearoa* (Lincoln University Press).

Smith, W.H.F. and Sandwell, D.T. (1997). Global sea floor topography from satellite altimetry and ship depth soundings. *Science 277*: 1956-1962.

Walters, R.A. (1987). A model for tides and currents in the English Channel and North Sea. *Advances in Water Resources 10*: 138–148.

Walters, R.A. (1992). A 3D, finite element model for coastal and estuarine circulation. *Continental Shelf Research 12*: 83–102.

Walters, R.A. (2002). Long wave resonance on the New Zealand coast. *NIWA Technical Report 109*, 32 p.

Walters, R.A., Goring, D.G., and Bell, R.G. (2001). Ocean tides around New Zealand. *New Zealand Journal of Marine and Freshwater Research 35*: 567–579.

Witter, R.C., Kelsey, H.M., and Hemhill-Haley, E. (2001). Pacific storms, El Niño and tsunamis: competing mechanisms for sand deposition in a coastal marsh, Euchre Creek, Oregon. *Journal of Coastal Research 17*, 563-583.

Wright, I.C. and Gamble, J.A. (1999). Southern Kermadec submarine caldera arc volcanoes (SW Pacific): caldera formation by effusive and pyroclastic eruption. *Marine Geology* 161, 207–227.

Wright, I.C., Gamble, J.A., and Shane, P.A. (in press). Submarine silicic volcanism of the Healy caldera, southern Kermadec arc (SW Pacific): I-volcanology and eruption mechanisms. *Bulletin of Volcanology*.

Table 1: Diagnostic characteristics of tsunami (after Goff et al, 2001b)

Diagnostic characteristics
• The deposit generally fines inland and upwards within the unit. Deposits often rise in altitude inland
• Each wave *can* form a distinct sedimentary unit, although this is not often recognised in the sedimentary sequence
• Distinct upper and lower sub-units representing runup and backwash can be identified
• Lower contact is unconformable or erosional
• Can contain intraclasts of reworked material, but these are not often reported
• Often associated with loading structures at base of deposit
• Particle/grain sizes range from boulders (up to 750 m^3), to coarse sand to fine mud. However, most deposits are usually recognised as anomalous sand units in peat sequences
• Generally associated with an increase in abundance of marine to brackish water diatoms, but reworking of estuarine sediments may simply produce the same assemblage
• Marked changes in foraminifera (and other marine microfossils) assemblages. Deeper water species are introduced with catastrophic saltwater inundation
• Pollen concentrations are often lower (diluted) in the deposit
• Increases in the concentrations of sodium, sulphur, chlorine, calcium and magnesium occur in tsunami deposits relative to under- and overlying sediments – indicates saltwater inundation and/or high marine shell content
• Individual shells and shell-rich units are often present (shells are often articulated)
• Often associated with buried vascular plant material and/or buried soil
• Shell, wood and less dense debris often found "rafted" near top of sequence
• Often associated with reworked archaeological remains (e.g. middens). In some cases occupation layers are separated by a palaeotsunami deposit

Table 2: Summary of palaeotsunami data (see Figure 1 for locations)

Date	Location	Comments	References
c.1450AD	Nationwide	❑ The 1450AD 'event' is most likely related to a number of tsunamis generated by a cluster of large earthquakes in the 15th Century	Goff and McFadgen, 2002
		• *Abel Tasman National Park* – up to 3.5km inland, primarily mud in sand	Goff and Chagué-Goff, 1999
		• *Archaeological sites* – almost ubiquitous signal of inundation found throughout the country	Goff and McFadgen, 2002
		• *Canterbury region* – Up to 2 km inland, sand	J. Goff, unpublished data
		• *Great Barrier Island/Far North* – up to at least 350m inland, runup over 32 masl, reworking of Maori ovens/midden sites	Nichol et al, 2002; in press
		• *Kapiti Is*. – over 200m inland, runup over 10 masl, saltwater inundation of environment	Goff et al., 2000
		• *Okarito* – over 2.5km inland, runup over 5 masl, destruction of nearshore vegetation	Goff et al., 2001c
		• *Palliser Bay* –over 3.5km inland, erosion of coast for about 1.5 km landward	Goff et al., 1998
c.1220AD	Nationwide	❑ Effects were similar in Abel Tasman National Park and on Kapiti Is. Using the 1450AD as a template, it is likely that the event is not preserved in Palliser Bay (see above) because this is an exposed coastline and the last event (1450AD) removed evidence of previous ones. Identification of this event in association with archaeological sites on the east coast suggests that this was also nationwide	Goff and Chagué-Goff, 1999 Goff et al., 2000 Goff et al., 1998 Goff et al., 2001a
c.950AD	Nationwide	❑ As per 1450AD, although probably smaller. No significant field evidence has been found, but it links with other seismic related events occurring at the time. It is probable that much evidence was destroyed by later events, or that the deposit is present but not picked up by the broad brush, low resolution analyses undertaken so far	Goff et al., 2001a Goff and McFadgen, 2002
c.500AD	Nationwide	❑ As per 950AD	Goff et al., 2001a Goff and McFadgen, 2002
c.200AD	Nationwide	❑ Probably related to a volcano-meteorological tsunami generated by the Taupo eruption, although seems to have occurred with some earthquake clustering. Similar to the 1450AD event	Goff and Chagué-Goff, 1999 Lowe and de Lange, 2000 Goff et al., 2000 Goff and McFadgen, 2002
c.2500BP	Nationwide	❑ Probably smaller than the 1450AD event, but larger than the possible 950AD and 500AD events. It is recorded in sediments of Abel Tasman National Park and Kapiti Is. Effects would have been similar to those reported for the 1450AD above, also appears to have affected Chatham Is.	Goff and Chagué-Goff, 1999 Goff et al., 2000 Goff et al., 2001a
c.3000BP	Wairoa, Kapiti Nationwide?	❑ If these events are near-synchronous, then it seems likely that this would be of nationwide coverage. It is probably similar to the 1450AD template. At Wairoa the deposit is poorly preserved and assumed to be relatively smaller than earlier events (below).	Goff et al., 2000 Chagué-Goff et al. 2002
c.4000BP	Canterbury	❑ Up to 2km inland, associated with mid-Holocene highstand?	J. Goff, unpublished data
c.5000BP	Wairoa, Kapiti Nationwide?	❑ As per 3000BP, but also found on Chatham Island.	Goff et al., 2000 Goff et al., 2001a
c.6300BP	Wairoa Nationwide?	❑ This was a large event, penetrating at least 2 km inland. Runup height is unclear because subsidence has taken place but probably about 15 masl.	Chagué-Goff et al. 2002 Chagué-Goff et al. 2002

BASIC RELATIONS BETWEEN TSUNAMIS CALCULATION AND THEIR PHYSICS–II

Zygmunt Kowalik
Institute of Marine Science, University of Alaska
Fairbanks, AK 99775, USA

ABSTRACT

Basic tsunami physics of propagation and run-up is discussed for the simple geometry of a channel. Modifications of a numerical technique are suggested for the long-distance propagation and for the nonlinear processes in tsunami waves. The principal modification is application of the higher order of approximations for the first derivative in space. Presently, tsunami calculations employ the high resolution 2D and 3D models for generation and runup processes, while propagation is resolved by the regular 2D models. Such approach requires boundary conditions which will seamlessly connect the high resolution calculations to the propagation models. These conditions are described with the help of the method of characteristics.

1. Introduction

This is the second part of the paper on relations between tsunami calculations and their physics (Kowalik, 2001, hereinafter, K01). The purpose is to consider modifications of numerical techniques used for the long-distance open ocean propagation and for the upslope propagation. While computing an open-ocean propagation at the resolution of 1 nautical mile (approximately 2km) the numerical dispersion slowly changes tsunami wave parameters by changing amplitude and generating the short dissipative waves. This is especially important for the long-distance deep-ocean propagation of the short-period waves (5min-15min period). To alleviate these numerical effects we suggest using of the higher order of approximations especially for the spatial derivative.

While tsunami wave starts to climb upslope towards the shore the nonlinear advective terms in the equations of motion and the nonlinear terms in the continuity equations start to play important role. Tsunami wave steepens up and starts to break into shorter waves. This dissipative process cannot be fully reproduced through the numerical means because it is connected to the short wave domain, which is not resolved by the applied numerical grid. In this domain the short waves of numerical origin occur along with the physical processes. Neither higher space resolution nor higher time resolution is completely rectifying this problem which starts in the subgrid domain. Application of the simple filter results in deleting the short numerical waves thus allowing to observe how tsunami wave changes while part of its energy is outflowing into the short wave during the tsunami wave breaking. Is this "remnant" tsunami wave is actually observed in nature or only in the computer models? Investigations in this paper and results given by Lynett et al. (2001) show that the physics of the nonlinear processes can be described by numerical solution but the numerical solution needs modifications to take into account the wide spectra of processes.

Applications of the different numerical approaches for the different ocean domains require boundary conditions which will seamlessly connect these domains. A problem to be considered is construction of semi-transparent boundaries. The boundary between oceanic and coastal domains should allow the signal arriving from the ocean to enter the coastal domain without any reflection or dissipation and afterwards when the signal is reflected by shoreline back towards the ocean it must cross the same boundary without any reflections as well. If, for example, such boundary is not completely transparent for tsunami which has entered coastal domain and a portion of the signal is reflected from the boundary back, tsunami will pump energy towards the shore causing permanent increase of the amplitude at the shore. The various conditions at the open boundaries are described with the help of the method of characteristics.

2. Numerical approximations for the spatial derivatives.

Consider the numerical solution of the equations of motion and continuity

$$\frac{\partial u}{\partial t} = -g\frac{\partial \zeta}{\partial x} \tag{1}$$

$$\frac{\partial \zeta}{\partial t} = -\frac{\partial}{\partial x}(Hu) \tag{2}$$

Solution of this system is usually searched by the two-time-level or the three-time-level numerical schemes (Kowalik and Murty, 1993a, Imamura, 1996). For construction of the space derivatives in the eqs. (1) and (2), a space staggered grid (Figure 1) is usually used (Arakawa C grid). The two-time-level numerical scheme

$$\frac{(u_j^{m+1} - u_j^m)}{T} = -g\frac{\zeta_j^m - \zeta_{j-1}^m}{h} \tag{3}$$

$$\frac{\zeta_j^{m+1} - \zeta_j^m}{T} = -\frac{(u_{j+1}^{m+1} H_{j+1} - u_j^{m+1} H_j)}{h} \tag{4}$$

is of the second order of approximation in space and only the first order in time. All notations are standard: u is velocity, ζ denotes sea level changes, t is time, x denotes horizontal coordinate, g is the Earth's gravity acceleration (g=981 cm s^{-2}), and H is depth.

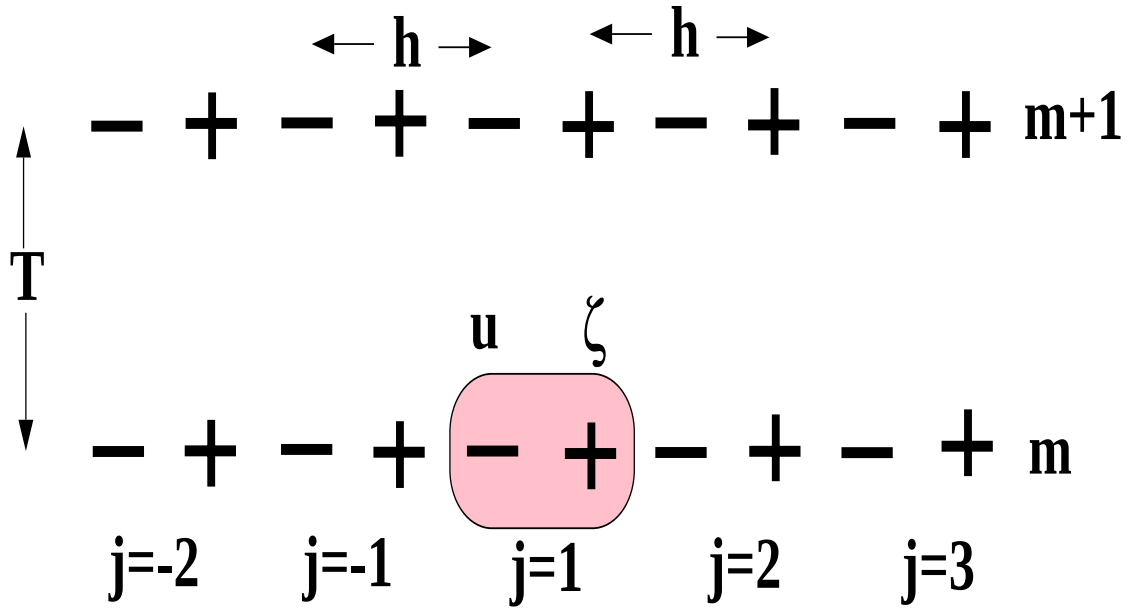

Figure 1
Space-time grid for the tsunami propagation. j is space index, m is time index.

The space-staggered grid given in Figure 1 is used to construct space derivatives in the above equations. Variables u (dashes) and ζ (crosses) are located in such a way that the second order of approximation in space is achieved. The depth is taken in the sea level points. The space step along the x direction is h. Index m stands for the time stepping and the time step is T. Let us consider a simple problem of a sinusoidal wave propagating over the long distance in the channel of the constant depth. At the left end of the channel a sinusoidal wave is given as

$$\zeta = \zeta_0 \sin(\frac{2\pi t}{T_p}) \tag{5}$$

Here the amplitude is ζ_0=100 cm, and the period T_p will be taken from 5 min to 0.5 hour range.

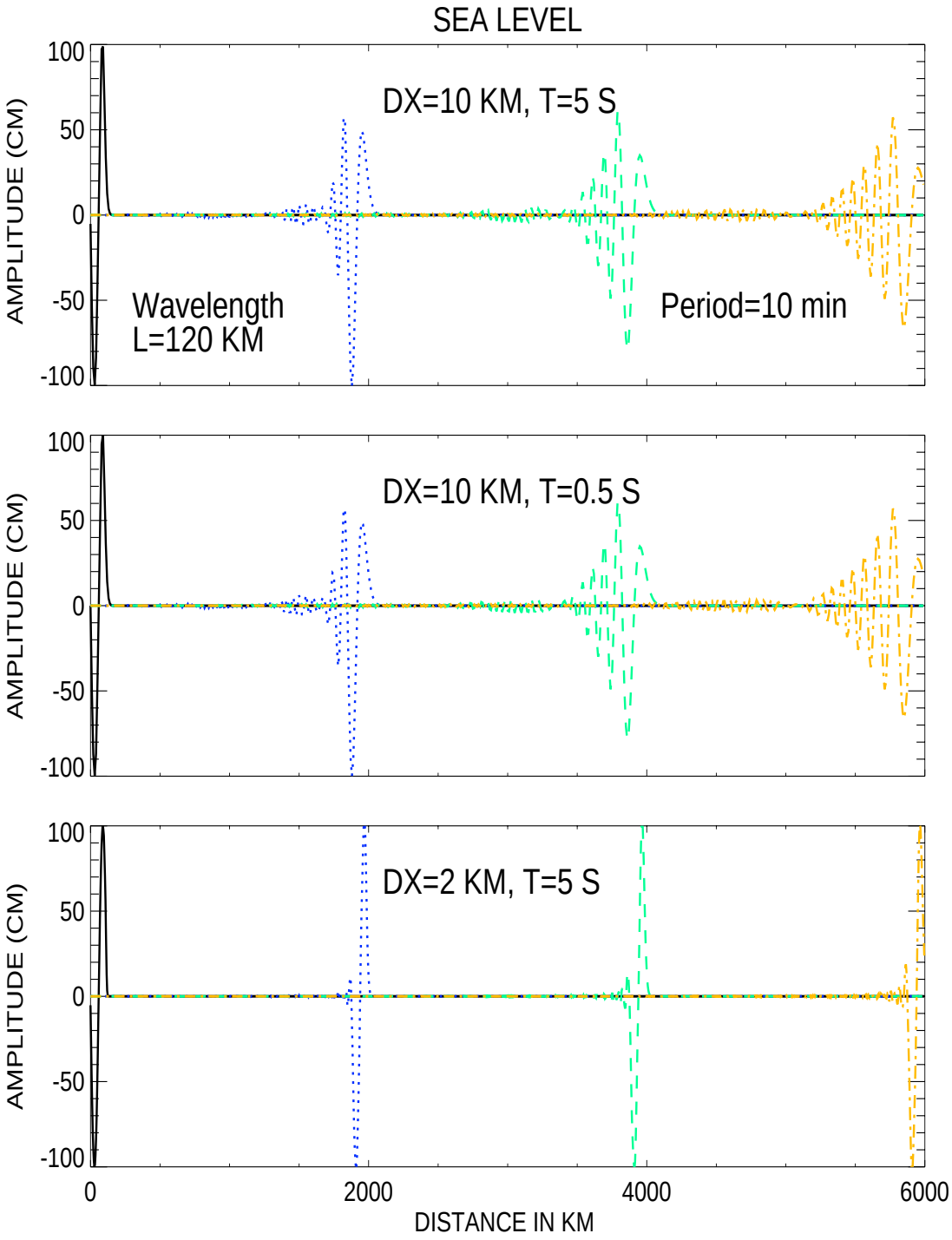

Figure 2

Propagation of the monochromatic wave of 10 min period along the channel of constant 4077 m depth. DX denotes spatial step and T is time step.

Propagation of this monochromatic wave toward the right end of the channel will be studied through eqs. (3) and (4). The right end of channel is open, and a radiating condition will be used so that the wave can propagate beyond the channel without reflection (see eq.(29) Sec. 5, and Reid and Bodine 1968). At the left end of the channel, eq (5) is applied for one period only; after that, the radiating condition is used as well. The channel is 6000 km long and 4077 m deep. The wave period under consideration is 10 min, which results in a 120-km wavelength. The time step of numerical integration will be taken equal to 5 s or 0.5 s. The initial space step is chosen equal to 10 km (close to $5'$ represented by gridded topography). The 10-km space grid sets 12 steps per wavelength (SPW). Such a resolution will slowly introduce numerical errors into reproduced waves. In Figure 2, results of computation are given for the space step of 10 km (SPW=12) and the time step 5 s (upper panel), for the space step of 10 km and the time step 0.5 s (middle panel), and for the space step of 2 km (SPW= 60) and the time step 5 s (bottom panel). The wave propagation from the left end has been depicted at distances of 2000 km, 4000 km, and 6000 km. The relatively poor space resolution in the upper and middle panels results in the wave damping along the channel.

At approximately 1500 km, the amplitude of the first wave became smaller than the amplitude of the second wave. Traveling wave train has a tail of secondary waves trailing behind the main wave. The shorter time step does not correct dispersive behavior (see the middle panel), only the shorter space step which increases the number of SPW, allows the nondispersive propagation. Dispersive numerical error is cumulative, i.e. for the longer travel distances it will become large enough to generate dispersive waves again. Therefore, the choice of the SPW index will depend on the propagation distance as well.

The time step is aimed at resolving the tsunami wave period and the space step at resolving wavelength. The above discussion shows that the encountered problems are related to the space resolution. This is because we are able to control time resolution but the spatial resolution depends on the resolution of the available bathymetric data. To improve solutions obtained by the numerical methods we shall apply higher order of approximations for the first derivatives in space. We start by constructing the space derivative for the sea level in the equation of motion. The central point (u point) located in the j grid point is surrounded by the two sea level grid points at the distance $h/2$ from the velocity point (see Fig. 1). Consider Taylor series in these points,

$$\zeta_{j+1/2} = \zeta_j = \zeta_j^u + \frac{\partial \zeta_j^u}{\partial x}\frac{h}{2} + \frac{1}{2}\frac{\partial^2 \zeta_j^u}{\partial x^2}(\frac{h}{2})^2 + \frac{1}{3!}\frac{\partial^3 \zeta_j^u}{\partial x^3}(\frac{h}{2})^3 + \frac{1}{4!}\frac{\partial^4 \zeta_j^u}{\partial x^4}(\frac{h}{2})^4 + O(h^5) \quad (6)$$

$$\zeta_{j-1/2} = \zeta_{j-1} = \zeta_j^u - \frac{\partial \zeta_j^u}{\partial x}\frac{h}{2} + \frac{1}{2}\frac{\partial^2 \zeta_j^u}{\partial x^2}(\frac{h}{2})^2 - \frac{1}{3!}\frac{\partial^3 \zeta_j^u}{\partial x^3}(\frac{h}{2})^3 + \frac{1}{4!}\frac{\partial^4 \zeta_j^u}{\partial x^4}(\frac{h}{2})^4 - O(h^5) \quad (7)$$

Along with Taylor series at the distance $h3/2$,

$$\zeta_{j+3/2} = \zeta_{j+1} = \zeta_j^u + \frac{\partial \zeta_j^u}{\partial x}\frac{3h}{2} + \frac{1}{2}\frac{\partial^2 \zeta_j^u}{\partial x^2}(\frac{3h}{2})^2 + \frac{1}{3!}\frac{\partial^3 \zeta_j^u}{\partial x^3}(\frac{3h}{2})^3 + \frac{1}{4!}\frac{\partial^4 \zeta_j^u}{\partial x^4}(\frac{3h}{2})^4 + O(h^5) \quad (8)$$

$$\zeta_{j-3/2} = \zeta_{j-2} = \zeta_j^u - \frac{\partial \zeta_j^u}{\partial x}\frac{3h}{2} + \frac{1}{2}\frac{\partial^2 \zeta_j^u}{\partial x^2}(\frac{3h}{2})^2 - \frac{1}{3!}\frac{\partial^3 \zeta_j^u}{\partial x^3}(\frac{3h}{2})^3 + \frac{1}{4!}\frac{\partial^4 \zeta_j^u}{\partial x^4}(\frac{3h}{2})^4 - O(h^5) \quad (9)$$

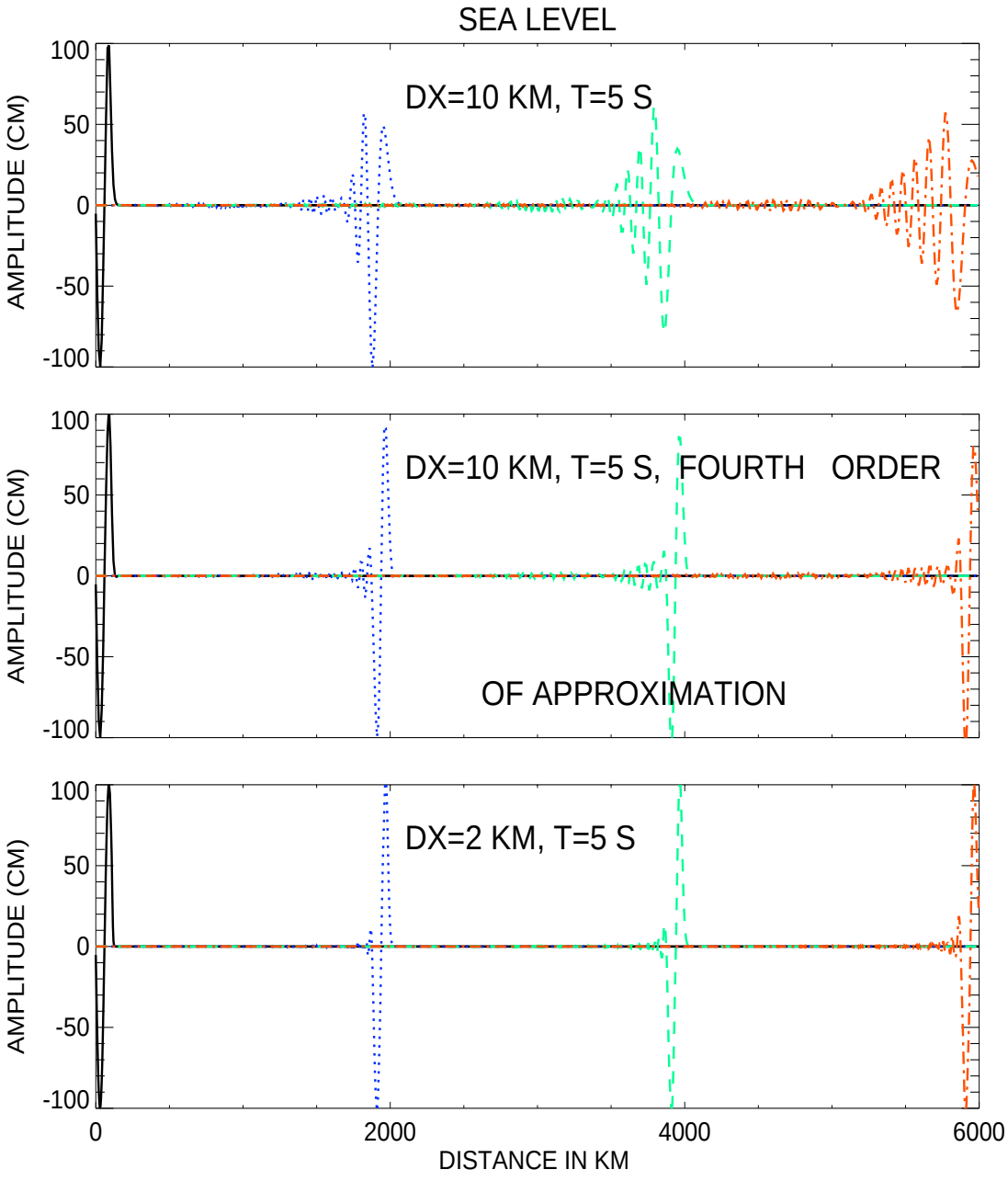

Figure 3

Propagation of the monochromatic wave of 10 min period along the channel of constant 4077 m depth. DX denotes spatial step and T is time step. Middle panel shows application of the higher order derivatives

Here ζ_j^u denotes the sea level in the u point. Space derivative for the sea level in (3) is

obtained by subtracting (7) from (6). Similar formula follows from (8) and (9), but with the longer space step of $3h$. The errors (the order of approximation) in both formulas, for the first derivative are proportional to the third derivatives. Thus by combining the two formulas the higher order formula can be constructed. The new formula for the first derivative of the sea level in the u point reads,

$$\frac{\partial \zeta}{\partial x} = [27(\zeta_j - \zeta_{j-1}) - (\zeta_{j+1} - \zeta_{j-2})]/24h + O(h^4) \tag{10}$$

Space derivative for the velocity in the continuity equation (2) can be constructed in the similar way by noticing that the central point for such derivative is the sea level and the space index should be moved to the right so that j ought to be substituted by $j+1$. Thus the derivative for the velocity in the ζ point reads

$$\frac{\partial}{\partial x}(Hu) = \{27[u_{j+1}(h_j + h_{j+1})/2 - u_j(h_j + h_{j-1})/2] -$$

$$[u_{j+2}(h_{j+2} + h_{j+1})/2 - u_{j-1}(h_{j-2} + h_{j-1})/2]\}/24h + O(h^4) \tag{11}$$

The propagation of the monochromatic wave described with the new derivatives is given in Fig. 3. This is repetition of the Fig. 2 with the middle panel resulting from application the new formulas. It shows essential improvement when compared against the results obtained with the second order derivatives (upper panel).

3. Propagation in sloping channel

We shall proceed to construct a simple algorithm for the propagation along the up-sloping channel as we did in the previous paper (K01). This numerical scheme allows us to investigate processes occurring across the shelf. We will be able to pinpoint the influence of friction and nonlinear terms on the process of propagation and dissipation and hopefully understand how numerical schemes change tsunami physics. Consider equation of motion and continuity along x direction:

$$\frac{\partial u}{\partial t} + u\frac{\partial u}{\partial x} = -g\frac{\partial \zeta}{\partial x} - \frac{ru|u|}{D} \tag{12}$$

$$\frac{\partial \zeta}{\partial t} = \frac{\partial}{\partial x}(Du) \tag{13}$$

Solution of this system will be searched through the two-time-level numerical scheme. The nonlinear (advective) term will be approximated by the upwind/downwind scheme. D in the above equations denotes the total depth $D = H + \zeta$.

The following numerical scheme is used to march in time:

$$\frac{(u_j^{m+1} - u_j^m)}{T} + up\frac{(u_j^m - u_{j-1}^m)}{h} + un\frac{(u_{j+1}^m - u_j^m)}{h}$$

$$= -g\frac{(\zeta_j^m - \zeta_{j-1}^m)}{h} + \frac{ru_j^m|u_j^m|}{0.5(D_j^m + D_{j-1}^m)} \tag{14}$$

Here: $up = 0.5(u_j^m + |u_j^m|)$, and $un = 0.5(u_j^m - |u_j^m|)$

$$\frac{\zeta_j^{m+1} - \zeta_j^m}{T} = -[(u_{j+1}^{m+1} 0.5(D_j^m + D_{j+1}^m) - u_j^{m+1} 0.5(D_{j-1}^m + D_j^m)]/h \qquad (15)$$

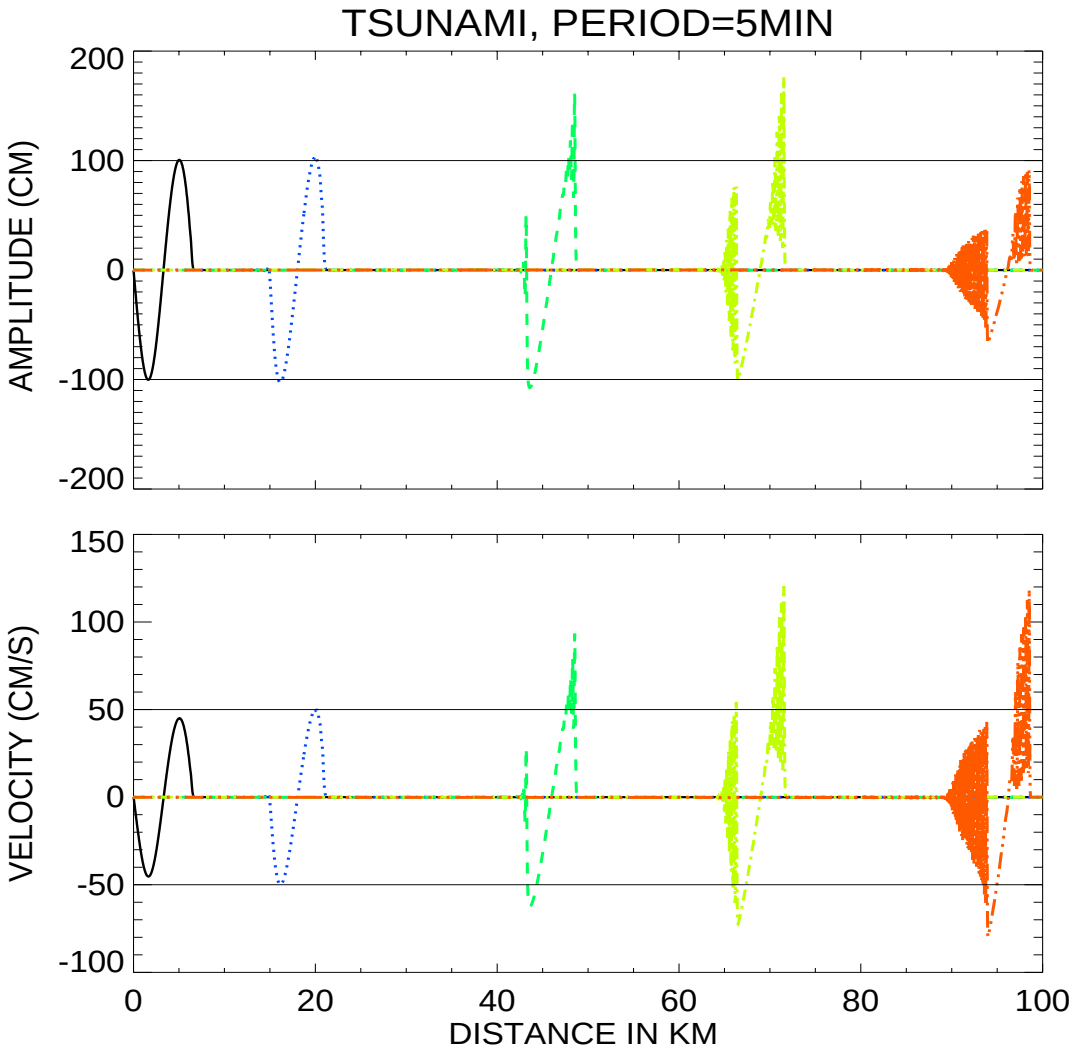

Figure 4
Amplitude (upper panel) and velocity (lower panel) of 5 min period wave. Advective term and bottom friction are included.

In this experiment the upsloping channel of 100 km length is considered. Depth is changing from 50 m at the entrance to 5 m at the end of the channel. We start by computing propagation of a 5 min period tsunami wave from the deep water towards the shallow water. Results we had obtained previously are depicted again in Fig.4. Again, it is important to notice the large disparity in the sea level and velocity. While the sea

level amplitude changes over a small range along the channel, velocity, on the other hand, displays much greater variations and is less prone to the dissipation. The wider range of changes in the velocity field offers better opportunity to compare models and observations. The comparison of the models against the sea level amplitude only, often show that the lack of the bottom friction results in an increase of the amplitude, but the results are not very different from the frictional models (Titov and Synolakis, 1998).

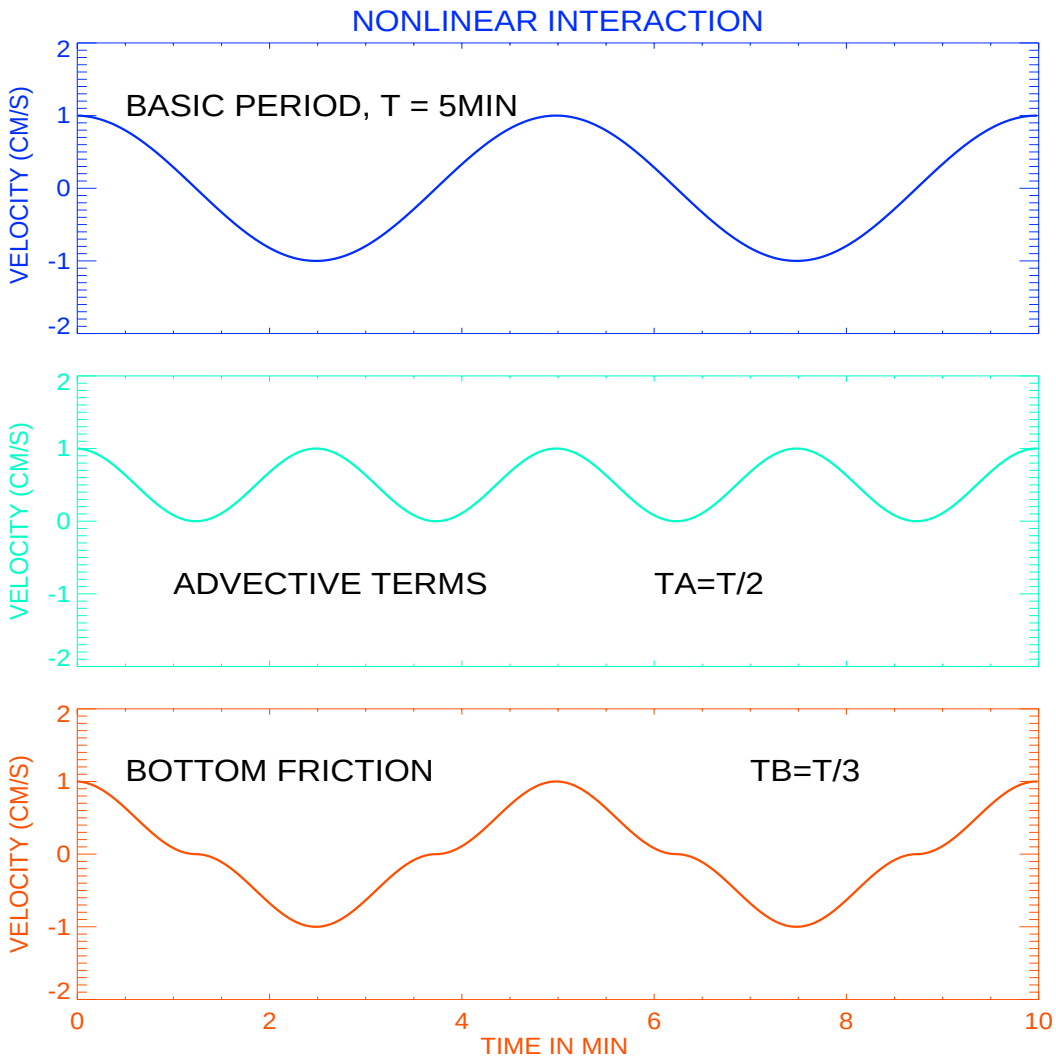

Figure 5

Velocity wave of the unit amplitude (upper panel). The nonlinear wave produced by the advective term (middle panel) and by the bottom friction (lower panel)

Here we investigate the wave breaking process in the upsloping channel. Is this true physical process of the long wave breaking or this is a numerical artifact? The period is 600 s and the time step 0.1 s, thus the temporal resolution is 6000SPP (step per period).

The wavelength is changing from approximately 7 km at the 50 m depth to 2 km at the 5 m depth. The latter is resolved with 25 m grid resulting in 80SPW, which is still an excellent resolution. Unfortunately, a simple notion of the spatial and temporal resolution needs to be reexamined since in the shallow water a strong nonlinear interaction occurs. This phenomenon should change our approach to analyzing the numerical stability of the basic set of equations, because previously we relied on the linear stability analysis only. Strong nonlinearities are often source of computational instabilities (Lewis and Adams, 1983). It follows from Fig.4 that even if the entire spectra of incident waves is limited to only one period the nonlinear interactions should result in the new periods and in the rectified current. The average velocity calculated over an incident wave period is not equal to zero, resulting therefore in the rectified currents. Let's consider a wave of the unit amplitude in velocity and of the 5 min period (Fig. 5, upper panel) and calculate the influence of the advective terms (middle panel) or the bottom friction terms (lower panel). The new period in the middle panel is 2.5 min, and in the bottom panel is 1.67 min. Generally, the wave of the period T generates through the advective terms the new oscillations whose periods are $T_A = T/2i$, where $i = 1, 2, 3, ...$ The new periods due to the bottom friction are $T_B = t/(2i + 1)$, where $i = 1, 2, 3, ...$ (Parker, 1991). It is of interest to notice that the amplitude of the secondary oscillations in the lower panel is significantly smaller that the amplitude of oscillations in the middle panel. Conclusion is that the advective mechanism more effectively transfers linear motion into the nonlinear motion. The process of breaking longer waves into shorter waves proceeds continuously, thus the waves shown in Fig. 5 will break into the shorter period waves as well. To test whether the short period waves are the part of physical phenomenon we carry out a simple experiment with an improved spatial resolution by taking step h=5m. The result of calculation is given in Fig. 6. In the upper panel for comparison the result with h=25 m is also shown.

The improvement in resolution (lower panel) leads to decreasing of the short wave oscillations. Therefore, we may conclude that the short wave oscillations is an computational artifact caused by the poor space resolution. The main source of nonlinear effects is advective term. To the advective term in eq. (14) the upwind method of the first order approximation in space is applied. The upstream approach is used for the stability reason. To deal with stability problems even with the higher order of approximation for the first derivatives (see Kowalik and Bang, 1987, Kowalik and Murty, 1993a) the upstream approach is needed. Construction of the first derivative can be carried out on the three-point or four-point stencil. For the three-point stencil the following construction can be used for the advective term,

$$u\frac{\partial u}{\partial x} \simeq up\frac{(3u_j^m - 4u_{j-1}^m + u_{j-2}^m)}{2h} + un\frac{(-u_{j+2}^m + 4u_{j+1}^m - 3u_j^m)}{2h} + O(h^3) \qquad (16)$$

Application of this approach to the advective term together with the higher order derivatives (10) and (11) for the remaining space derivatives leads again to the improved results shown in the lower panel of Fig. 7.

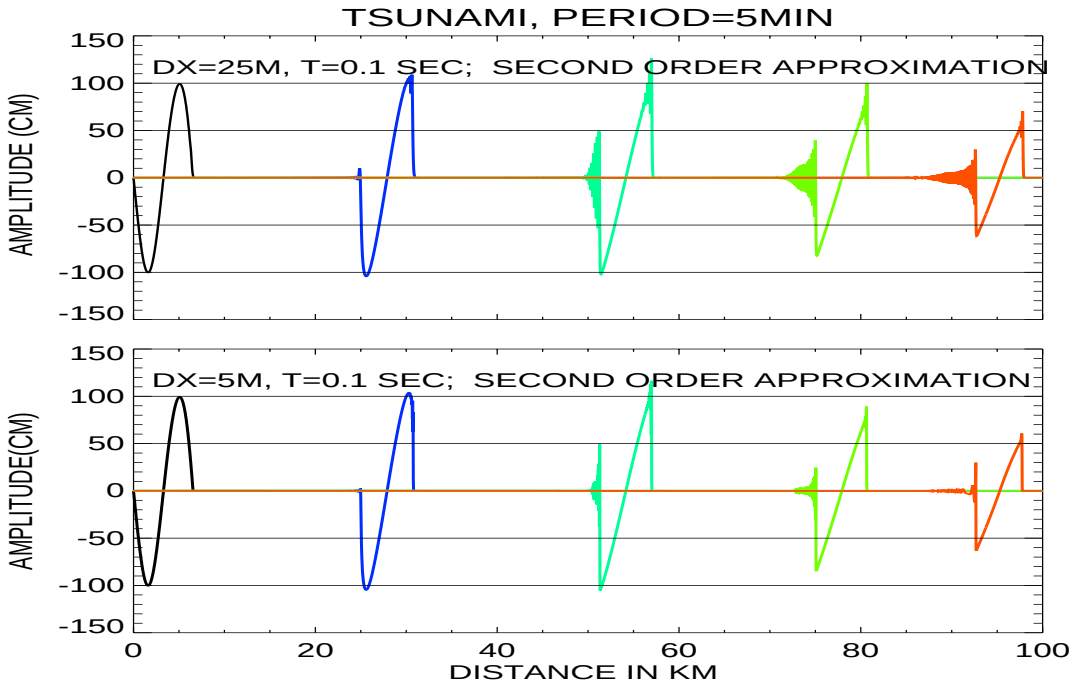

Figure 6

Wave traveling in upsloping channel. Solution obtained by eqs. (14) and (15). Upper panel: space step 25 m, lower panel: space step 5 m.

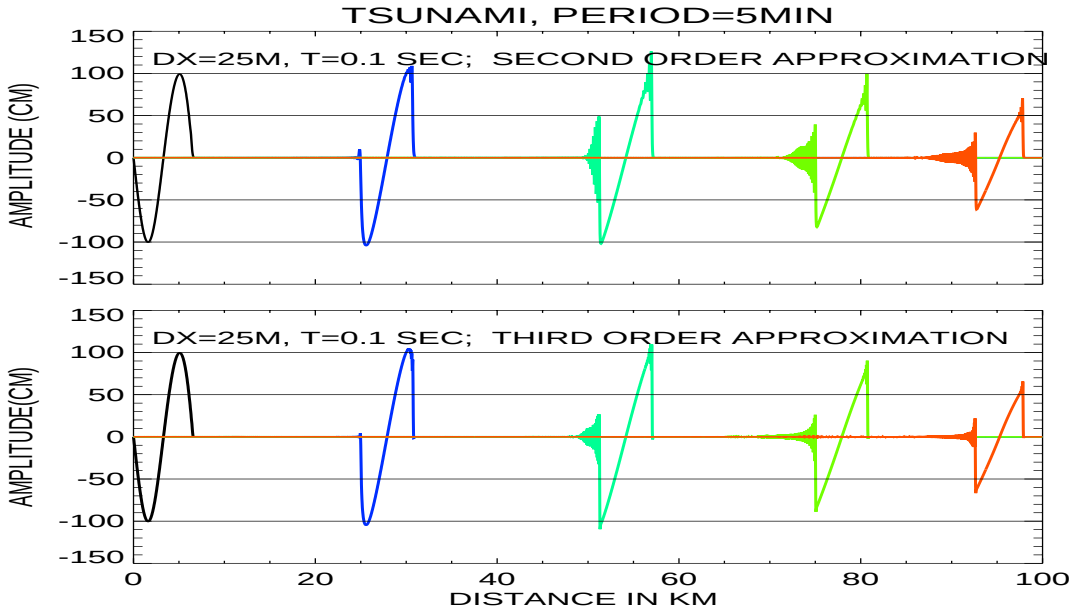

Figure 7

Wave traveling in upsloping channel. Upper panel: solution by eqs. (14) and (15), lower panel: solution by the third order approximation

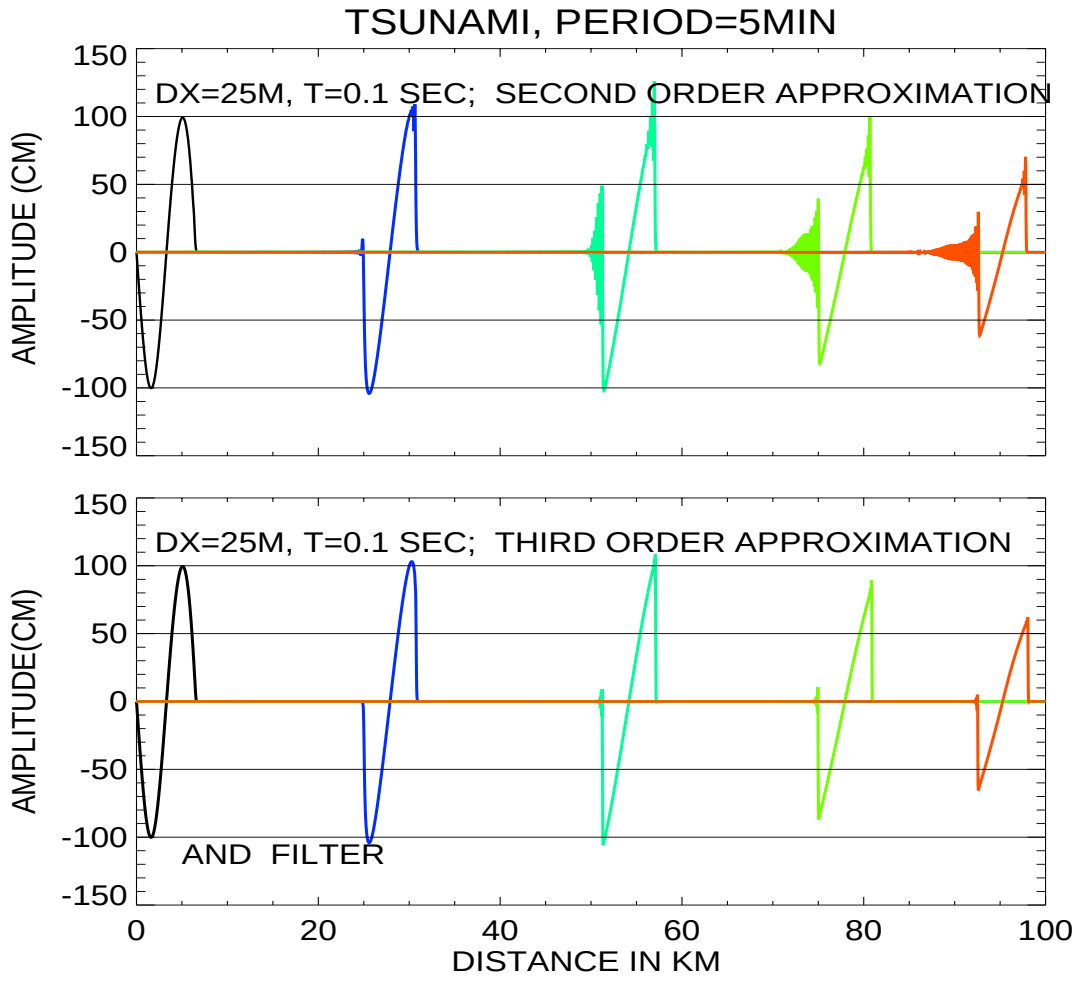

Figure 8
Wave traveling in upsloping channel. Upper panel: solution by eqs. (14) and (15), lower panel: solution by the third order approximation and space filter

Conclusion from the above experiments is that the parasitic short wave oscillations can be deleted through an application of the high spatial and temporal resolutions. A somewhat different and easier solution is application of a simple space filter. It is applied only to the computed velocity. The new velocity u_j^{m+1} is filtered in the following manner,

$$UN(J) = u_j^{m+1} * (1 - ALP) + 0.25 * (u_{j-1}^{m+1} + 2. * u_j^{m+1} + u_{j+1}^{m+1}) * ALP \qquad (17)$$

The filter parameter $ALP = 0.005$. The computation carried out with the high order derivatives and the above filter are shown in the lower panel of Fig. 8

4. Run-up in channel

We use here the algorithm previously given in K01, see also Kowalik and Murty, (1993b). The equation of motion is solved by (14), while the continuity equation is approximated by the upwind/downwind approach as well. This approach introduced by Mader (1986) makes equation of continuity quite stable at the boundary between wet and dry domains. The following numerical scheme is used to march in time for the equation of continuity:

$$\frac{\zeta_j^{m+1} - \zeta_j^m}{T} = -(upj1 \times D_j^m + unj1 \times D_{j+1}^m - upj \times D_{j-1}^m - unj \times D_j^m) \qquad (18)$$

In the above equation:

$$upj1 = 0.5(u_{j+1}^{m+1} + |u_{j+1}^{m+1}|) \quad \text{and} \quad unj1 = 0.5(u_{j+1}^{m+1} - |u_{j+1}^{m+1}|)$$

$$upj = 0.5(u_j^{m+1} + |u_j^{m+1}|) \quad \text{and} \quad unj = 0.5(u_j^{m+1} - |u_j^{m+1}|)$$

To simulate the run-up and run-down, the variable domain of integration is established after every time step by checking whether the total depth is positive. This was done through a simple algorithm proposed by Flather and Heaps (1975) for the storm surge computations. To answer whether u_j is a dry or wet point, the sea level is tested at this point;

$$\begin{cases} u_j \textit{ is wet point}, & \text{if } 0.5(D_{j-1} + D_j) \geq 0; \\ u_j \textit{ is dry point}, & \text{if } 0.5(D_{j-1} + D_j) < 0 \end{cases} \qquad (19)$$

Figure 9, middle and lower panels, describes an experiment in which 15 min and 30 min period waves of 1 m amplitude are continuously generated at the open end of the channel.

After this signal is reflected from the sloping boundary, a standing wave is settled in the constant bottom domain. One can glean from this figure that the runup for the 15 min period is much bigger than the runup for the 30 min. Such growth usually show conditions close to the resonance. The sea level distribution in the channel depends strongly on the open boundary condition used for the computation. Setting only velocity or sea level at the open boundary may generate an additional error. The boundary condition must be semi-transparent. With the help of such boundary condition we should be able to set required sea level (or velocity) at the boundary and when the incident wave reflects from a shore and arrives to the open boundary it should cross the boundary without any reflections. These boundary conditions are discussed in the next sections.

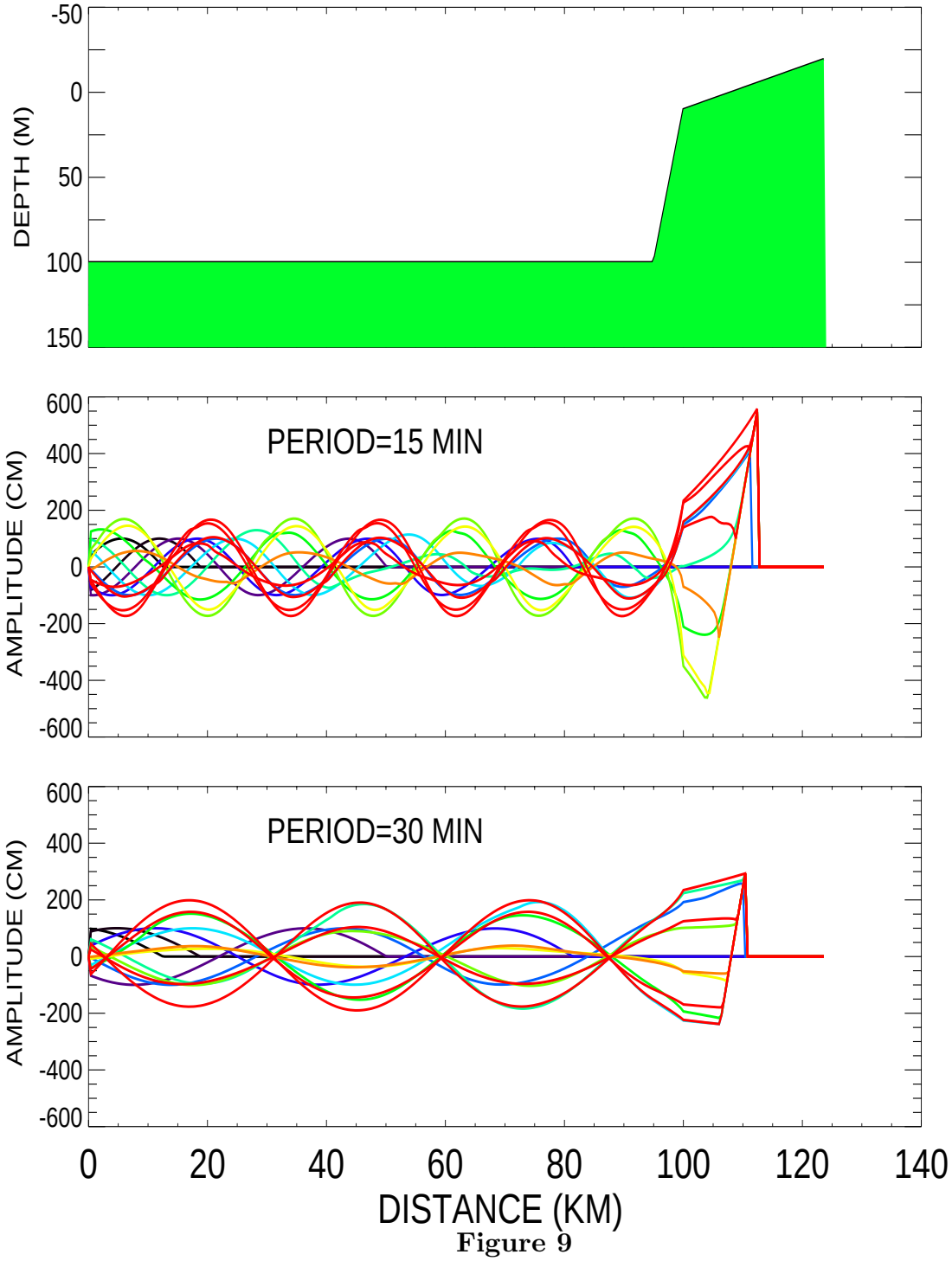

Figure 9

Upper panel: depth distribution. Propagation of 1 m amplitude wave: Middle panel: 15 min period, lower panel: 30 min period.

5. Boundary conditions for the tsunami problems

Presently, to calculate tsunami generation and runup the high resolution 2D or 3D models are used, while the open ocean physics is well resolved by 2D models. To construct a boundary condition for connecting the propagation and generation domains let's consider first a simple flow in a channel described by eqs. (1) and (2).

Introducing solution in the form $(u, \zeta) = (u_0, \zeta_0)\Phi(x - ct)$ into these equations gives rise to a simple set

$$-cu_0 + g\zeta_0 = 0 \tag{20}$$

$$Hu_0 - c\zeta_0 = 0, \tag{21}$$

whose solution defines the well known dispersion relation $c = \pm\sqrt{(gH)}$.

Solutions to eqs.(1) and (2) can be written now as superposition of two waves traveling into positive and negative directions along the x axis,

$$\zeta = \zeta_0^+\Phi(x - ct) + \zeta_0^-\Phi(x + ct) \tag{22}$$

$$u = u_0^+\Phi(x - ct) + u_0^-\Phi(x + ct) \tag{23}$$

Through eq.(20) and (21) the velocity amplitudes are related in the following way to the sea level amplitudes

$$u_0^+ = \sqrt{\frac{g}{H}}\zeta_0^+ \qquad \text{and} \qquad u_0^- = -\sqrt{\frac{g}{H}}\zeta_0^- \tag{24}$$

With this substitution eq.(23) reads,

$$u = \sqrt{\frac{g}{H}}\zeta_0^+\Phi(x - ct) - \sqrt{\frac{g}{H}}\zeta_0^-\Phi(x + ct) \tag{25}$$

Combining eqs.(22) and (23) the two dependent variables u and ζ are expressed by two disturbances $\zeta_0^+\Phi(x - ct)$ and $\zeta_0^-\Phi(x + ct)$ which we denote as Φ_+ and Φ_-. Through eqs.(22) and (25) these functions are expressed as

$$\Phi_+ = \frac{\zeta + u\sqrt{H/g}}{2} \tag{26a}$$

$$\Phi_- = \frac{\zeta - u\sqrt{H/g}}{2} \tag{26b}$$

The Φ_+ is a function of $x - ct$, therefore it must be constant along any line $x - ct$=constant. Such line is called characteristic and speed c is the slope of the characteristic (Abbot and Minns, 1998, Durran, 1999). In the finite difference domain a characteristic located between two spatial grid points at the old time step can be followed to predict the value of Φ_+ at the new time step. Similar conclusion can be deduced with respect to Φ_-.

The variables Φ_+ and Φ_- can be also used to construct two equations instead of eqs. (1) and (2),

$$\frac{\partial \Phi_+}{\partial t} + c\frac{\partial \Phi_+}{\partial x} = 0 \tag{27}$$

$$\frac{\partial \Phi_-}{\partial t} - c\frac{\partial \Phi_-}{\partial x} = 0 \tag{28}$$

These will better serve for the boundary condition construction since the values of Φ_+ and Φ_- are preserved along characteristics.

Consider, the wave propagation in a channel with the left end located at $x = 0$ and the right end at the distance $x = L$. From the left end enters a wave denoted as Φ_+, it propagates towards the right end. If the right boundary ought to be transparent to this wave the requirement is that there will be no reflection, or $\Phi_- = 0$. From eq.(26b) it follows that the sea level at the right end of the channel is

$$\zeta = u\sqrt{H/g} \tag{29}$$

Similarly, if the left end of channel ought to be transparent for an incoming wave, eq. (26a) will prescribe the sea level under condition that $\Phi_+ = 0$

$$\zeta = -u\sqrt{H/g} \tag{30}$$

Problem to solve is a construction of semi-transparent boundaries, when e.g., at the left-hand boundary a permanent signal is generated and the right-hand boundary is the reflective one. A signal, reflected from the right boundary when arriving to the left boundary must find the way out because if this boundary is not transparent the reflected signal will pump energy causing permanent increase of the amplitude in the channel. To this purpose, can serve eq. (26a), assuming that incoming wave from the left boundary is constant $\Phi_+ = Const$, the relations between amplitude and velocity follows. There are a few variations of this approach e.g., setting sea level at the left boundary as a constant and calculating Φ_+ and Φ_- along characteristics in proximity to the boundary and afterwards inserting this values for the boundary conditions to calculate velocity from eq.(23).

In many applications, while going from the larger-scale domain to the smaller-scale, the open boundary for the smaller domain are taken from the larger scale computations or observations. Suppose at the left-hand boundary the sea level (ζ_b) and velocity (u_b) are given either from measurements or computations. The incoming value of the Φ_+ is defined as

$$\Phi_+ = \frac{\zeta_b + u_b\sqrt{H/g}}{2} \tag{31}$$

and for the smooth propagation into domain this value ought to be equal to the invariant specified inside computational domain in the close proximity to the boundary

$$\Phi_+ = \frac{\zeta + u\sqrt{H/g}}{2} \tag{32}$$

or,

$$\zeta = \zeta_b + (u_b - u)\sqrt{H/g} \tag{33}$$

Some understanding of the above condition can be gleaned by comparison to the radiation conditions given by eqs. (29) and (30). Generally eq.(33) requires that at the boundary, calculated variables in the smaller domain be equal to the measured (or input variables). One cannot expect this condition to be fulfilled at the initial stage of a computation, especially when the computation start from zero velocity. The second term at the right-hand-side of eq.(33) is actually a radiation condition, which radiates difference between prescribed and computed velocity. When stationary conditions will be achieved the difference of velocity will be close to zero. Condition (33) is often used to establish open boundary condition for the tidal computations (Flather, 1976). The usefulness of eq.(33) for the transient tsunami processes requires further testing.

6. Numerical implementation of the boundary condition

Fig. 10 depicts grid distribution at the left-hand boundary. Two-time level numerical scheme is considered. Both sea level and velocity are having the same space index. Let's start by considering radiation boundary condition defined for the velocity. Here a simple implementation of eq.(30) reads,

$$u^{m+1} = -\zeta_1^{m+1}\sqrt{g/H} \tag{34}$$

The question to be answered is that eq.(34) is actually valid along the characteristic and not at the grid points. First, it is useful to notice that this radiating condition is also fulfilled by the equation for the sea level

$$\frac{\partial \zeta}{\partial t} - c\frac{\partial \zeta}{\partial x} = 0 \tag{35}$$

and thus the value of the sea level is constant along the characteristic which propagates from the old time (m) into the new time $(m+1)$ domains as shown in Fig. 10 by dashed line. The distance $dx = cT$, where c denote phase velocity and T is time step. The sea level at the old time step is defined at the point p on the characteristic,

$$\zeta_p = \frac{\zeta_1^m(h - dx) + \zeta_2^m dx}{h} \tag{36}$$

This sea level is equal to the sea level at the new time step ($\zeta_1^{m+1} = \zeta_p$), and since $dx = cT$, and time step and space step are given; denoting cT/h as γ, the above equation can be written as,

$$\zeta_1^{m+1} = \zeta_1^m(1 - \gamma) + \zeta_2^m\gamma \tag{37}$$

Eq.(37) can be introduced into (34) to calculate velocity. Notice that this velocity is defined in the sea level point ($j = 1$). Calculations show that actually (34) works quite well even if the variables are defined in the grid points and not along the characteristics.

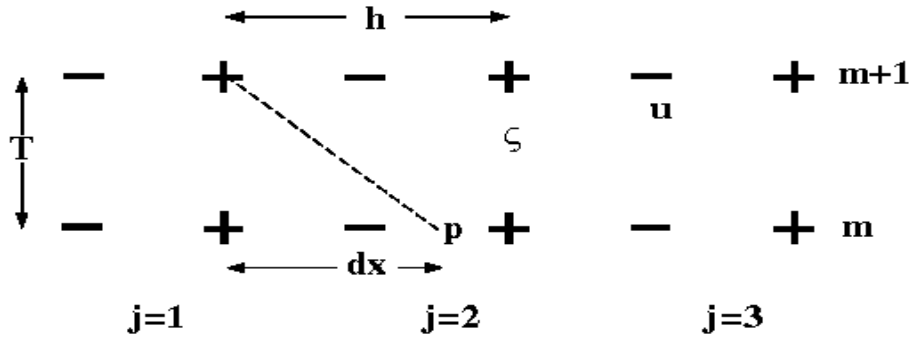

Figure 10

The boundary conditions defined through the modeling or observations require also smooth transition between conditions and computed variables. To this purpose serves well eq.(33); at the left boundary it can be written as (assuming sea level is prescribed at the j=1 grid point and velocity at the j=2 grid point),

$$\zeta_1^{m+1} = \zeta_b^{m+1} + (u_b^{m+1} - u_2^{m+1})\sqrt{H/g} \tag{38}$$

The major problem arises when only one variable is given at the open boundary: sea level or velocity. With such condition an incoming characteristic is not fully defined, therefore the above relation cannot be applied. It is easy to start computation with the prescribed sea level but when the reflected wave arrives to the open boundary and its magnitude differs from the open boundary value, the energy build up ensue resulting in an instability. Several solutions are feasible but none is resolving the problem completely. Generally, a difference between the prescribed sea level magnitude at the boundary and the sea level generated by the reflected wave at the same boundary is due to an initial adjustment problem or due to transient character of the signal. The prescribed boundary condition should actually include both incoming and outgoing signal. One possible solution for arriving at the stationary signal, is to introduce the radiating mechanism into a boundary condition and slowly remove this mechanism in time. Assume, at the left boundary the amplitude is prescribed as $\zeta_1^{m+1} = a\cos\omega(m+1)T$, now introducing accordingly to eq.(30) a radiating signal, the boundary condition at the left boundary reads,

$$\zeta_1^{m+1} = a\cos\omega(m+1)T - u_2^{m+1}\sqrt{H/g} \tag{39}$$

The second term at the right-hand-side of the above equation ought to be slowly removed in time after the initial adjustment process is over. If only the sea level (ζ_b^{m+1}) is given

at the boundary a different approach can be worked out starting from eq.(38). The new boundary value (ζ_1^{m+1}) at the same grid point can be calculated by the radiation condition, using, e.g., eq.(37). This sea level will differ from prescribed boundary value ζ_b^{m+1}. The difference may be used to calculate a correction for the boundary value of velocity at the point $j = 2$. We rewrite eq.(38) as

$$u_{2,c}^{m+1} = u_2^{m+1} + \sqrt{g/H}(\zeta_b^{m+1} - \zeta_1^{m+1}) \tag{40}$$

Velocity u_2^{m+1} has been computed in the regular way, i.e., by application of ζ_b^{m+1} as the boundary value.

Acknowledgments

This study was supported by the Arctic Region Supercomputing Center at the University of Alaska Fairbanks. I am indebted to my students Juan Horrillo and Elena Suleimani for their help and discussions throughout the work.

References

Abbot, M.B. and A.W. Minns. 1998. *Computational Hydraulics.* Ashgate, Aldershot, 557pp.

Durran, D.R. 1999. *Numerical Methods for Wave Equations in Geophysical Fluid Dynamics.* Springer, 465pp.

Flather, R.A. 1976. A tidal model of the north-west European continental shelf. *Mem. Soc. R. Sci. Liege*, **6**, 141–164.

Flather, R.A. and Heaps, N.S. 1975. Tidal computations for Morecambe Bay. *Geophys. J. Royal Astr. Soc.*, **42**, 489-517.

Imamura F. 1996. Review of tsunami simulation with a finite difference method. In *Long-Wave Runup Models*, H.Yeah, P. Liu and C. Synolakis, Eds, World Scientific, 25–42.

Kowalik, Z. 2001. Basic relations between tsunami calculation and their physics, *Science of Tsunami Hazards*, **19**, 2, 99–115.

Kowalik, Z. and I. Bang. 1987. Numerical computation of tsunami run-up by the upstream derivative method.*Science of Tsunami Hazards*, **5**, 2, 77–84.

Kowalik, Z. and Murty, T.S. 1993a. *Numerical Modeling of Ocean Dynamics*, World Scientific, 481 pp.

Kowalik, Z. and Murty, T.S. 1993b. Numerical simulation of two-dimensional tsunami runup. *Marine Geodesy*, **16**, 87–100.

Lewis, C.H. III and Adams, W.M. 1983. Development of a tsunami-flooding model having versatile formulation of moving boundary conditions. *The Tsunami Society MONOGRAPH SERIES*, No.**1**, 128 pp.

Lynett, P.J.,Tso-Ren Wu and P. L.-F. Liu. 2001. Modeling wave runup with

depth-integrated equations. Submitted to Coastal Engineering.

Mader, C. L. 1986. *Numerical Modeling of Water Waves*, Univ. Calif. Press, Berkeley, Los Angeles, 206 pp.

Parker, B. B. 1991. The relative importance of the various nonlinear mechanisms in a wide range of tidal interactions (Review). In: *Tidal Hydrodynamics*, B. B. Parker, Ed., Wiley and Sons, 237–268.

Reid, R.O. and B.R. Bodine. 1968. Numerical model for storm surges in Galveston Bay. *J. Waterway Harbour Div.*, **94**(WWI), 33–57.

Titov, V.V. and Synolakis, C.S. 1998. Numerical modeling of tidal wave runup. *J. Waterway, Port, Coastal and Ocean Eng.*, **124**, 4, 157–171.